Impacts of the 1900-1974 increase in anthropogenic aerosol emissions from North America and Europe on Eurasian summer climate

The DOI for this manuscript is doi: 10.1175/JCLI-D-17-0850.1

Undorf, S., M. Bollasina, and G. Hegerl, 2018: Impacts of the 1900-1974 increase in anthropogenic aerosol emissions from North America and Europe on Eurasian summer climate. J. Climate. doi:10.1175/JCLI-D-17-0850.1, in press.

Impacts of the 1900-1974 increase in anthropogenic aerosol emissions from North America and Europe on Eurasian summer climate

S. Undorf*, M. A. Bollasina, and G. C. Hegerl

School of GeoSciences, Crew Building, The University of Edinburgh, The King's Buildings, Alexander Crum Brown Road, Edinburgh, EH9 3FF, UK.

* *Corresponding author address:* School of GeoSciences, Crew Building, The University of Edinburgh, The King's Buildings, Alexander Crum Brown Road, Edinburgh, EH9 3FF, UK.

E-mail: s.undorf@ed.ac.uk

ABSTRACT

The impact of North American and European (NAEU) anthropogenic aerosol emissions on Eurasian summer climate during the twentieth century is studied using historical single- and all-forcing (including anthropogenic aerosols, greenhouse gases, and natural forcings) simulations from the Coupled Model Intercomparison Project Phase 5 (CMIP5). Inter-model agreement on significant linear trends during a period of increasing NAEU sulphate emissions (1900-1974) reveals robust features of NAEU aerosol impact, supported by opposite changes during the subsequent period of decreasing emissions. Regionally, these include a large-scale cooling and associated anticyclonic circulation as well as a narrowing of diurnal temperature range (DTR) over Eurasian mid-latitudes. Remotely, NAEU aerosols induce a drying over the western African and northern Indian monsoon regions, and a strengthening and southward shift of the sub-tropical jet consistent with the pattern of temperature change. Over Europe, the temporal variations of observed temperature, pressure, and DTR tend to agree better with simulations that include aerosols. Throughout the twentieth century, aerosols are estimated to explain more than a third of the simulated inter-decadal forced variability of European near-surface temperature, and more than half between 1940 and 1970. These results highlight the substantial aerosol impact on Eurasian climate, already identifiable in the first half of the twentieth century. This may be relevant for understanding future patterns of change related to further emission reductions.

1. Introduction

Increasing awareness and concern about the risks associated with the unfolding of climate change, including changes in droughts and floods associated with shifts in precipitation patterns, have posed considerable demand for credible climate projections at regional scale. Robust information on regional impacts is crucial to be better prepared to manage and mitigate the impacts on our society and the environment, including agriculture, energy, and water resources. Despite their importance, reliable projections of regional climate change still remain a major challenge (IPCC, 2013).

Anthropogenic aerosols can drive changes in global and regional climate by impacting both the energy and water cycles; yet, despite progress in the last decade, aerosols have remained the dominant contributor to the uncertainty in total anthropogenic forcing over the industrial era in the last three IPCC reports (IPCC, 2013). Uncertainties in quantifying the aerosol impact on climate also hinder our ability to estimate the greenhouse gas (GHG) contribution to the recent global temperature change (Hegerl et al., 1997; Stott and Jones, 2012; Ribes and Terray, 2013; Gillett et al., 2013; Schurer et al., 2017). Although the IPCC (2013) assessed it as 'extremely likely' that more than half of the observed warming since the mid-twentieth century was due to human influences, the uncertainties in the separate effects of greenhouse gases and aerosols are much larger. As emissions of GHGs and aerosols follow different pathways in the future, separation of their respective effects is essential for improving confidence in climate projections for the 21st century.

At global scale, aerosols are estimated to exert a net negative effective radiative forcing of -0.9 W/m^2 (-1.9 to -0.1 W/m^2 at 90% confidence level) on present-day climate, offsetting part of the GHG-induced warming (Myhre et al., 2013). This negative radiative forcing results from pertur-

bation of the climate system through radiative and cloud micro-physical effects (aerosol-radiation and aerosol-cloud interactions, respectively; Boucher et al. (2013)), the relative magnitudes of which vary across aerosol species. In the direct effect (Charlson et al., 1992), aerosols scatter and absorb mainly solar radiation and thus modify the surface and atmospheric temperature distributions. The atmospheric heating thereby caused by strongly absorbing aerosols like black carbon can cause cloud changes by altering the surface energy budget and static stability as well as by cloud evaporation (burn-off); these changes are often referred to as the semi-direct effect (Hansen et al., 1997). Sulphate aerosols, on the other hand, scatter solar radiation, and are additionally efficient cloud condensation nuclei (CCN), which in turn affects cloud micro-physical properties and precipitation processes – the cloud albedo (first indirect) (Twomey, 1977) and the cloud lifetime (second indirect) effect (Albrecht, 1989). Non-linearities in these indirect aerosol effects, caused by saturation effects in the cloud-aerosol interactions, can cause aerosols to be more important in a more pristine atmosphere (e.g. Carslaw et al. (2013)).

Being emitted mainly by fossil fuel and biomass burning sources, present-day global atmospheric levels of sulphate, organic carbon, and black carbon are substantially larger than those at pre-industrial times. Historical changes, however, have neither been linear nor spatially homogeneous. They result mainly from a combination of changes over two macroregions: Emissions from North America and Europe (NAEU) increased steadily from pre-industrial times to the peak in the 1970s, when air quality legislation led to their reduction. Asian emissions, in contrast, started to rapidly increase in the 1950s as a result of rapid economic development and have been increasing ever since (Lamarque et al., 2010; Hoesly et al., 2017). These geographical differences in the emission time series, combined with the short lifetime of aerosols in the atmosphere, result in spatially and temporally heterogeneous distributions and higher concentrations around the source regions. The global mean impact of aerosols is therefore not necessarily representative of regional climate

responses, which can be substantial (e.g. Ramanathan et al. (2001)) even when the magnitude of global forcing remains relatively small.

Numerous studies have suggested that anthropogenic aerosols had an important impact on the twentieth century climate over various regions (Boucher et al., 2013; Bindoff et al., 2013). Emissions of aerosols from human activities predominantly located in the northern hemisphere (NH) have for instance been linked to a southward shift of the Inter-Tropical Convergence Zone since the early 1900s by muting the warming of the northern hemisphere relative to the southern hemisphere (Chiang and Friedman, 2012; Rotstayn and Lohmann, 2002; Hwang et al., 2013). Aerosols have been shown to have played a predominant role in the decrease of northern hemisphere monsoon precipitation (Polson et al., 2014), as well in weakening its regional components over East Asia (Li et al., 2016; Guo et al., 2013), South Asia (Bollasina et al., 2013; Undorf et al., 2018), and North West Australia (Rotstayn et al., 2012). Furthermore, aerosols were found to have contributed to the decrease of precipitation in West Africa (Ackerley et al., 2011; Dong et al., 2014), to cause tropical contraction (Allen and Ajoku, 2016), and to have modulated the Atlantic multi-decadal circulation and North Atlantic storms (Booth et al., 2012; Dunstone et al., 2013). Aerosol reductions in recent decades might have amplified Arctic temperature increase and sea-ice loss (Acosta Navarro et al., 2016). Yet, many of these findings are associated with large uncertainties and are, at times, controversial, resulting in vivid discussions across the scientific community. IPCC (2013) noted that the "lack of agreement across studies prevents generalization of findings to project aerosol-induced changes in regional atmospheric circulation or precipitation in the near term".

This is also true for studies focused on European climate, where changes in surface temperature and diurnal temperature range (DTR) have been related to aerosol-induced shift in the surface solar radiation regime from dimming to brightening (Wild et al., 2007; Makowski et al., 2008, 2009). DTR is a measure of high-frequency temperature variability and is not only important for

climate impacts as diverse as crop yields (Lobell et al., 2007) and human mortality and morbidity (Kim et al., 2016), but has also been suggested to be a useful indicator to separate aerosol and GHG forcing (Schnur and Hasselmann, 2005; Wild et al., 2007): Through reducing surface solar radiation, aerosols are expected to reduce maximum (Tmax) more than minimum (Tmin) temperature, causing a decrease in DTR, while GHG interact with outgoing long-wave radiation and are thus expected to impact Tmax and Tmin equally (although a preferred response of TMIN to GHG warming has also been suggested (Rohde et al., 2013a)). Other studies found the recent reduction in aerosols to have increased the frequency of light precipitation events despite no changes in total precipitation in observations (Stjern et al., 2011) and an increase in the ratio between convective to stratiform precipitation in a GCM (Stjern and Kristjánsson, 2015). Complex interactions underpin also the relationship between European aerosol loading and the North Atlantic Oscillation (Chiacchio et al., 2011; Pausata et al., 2014).

Located upstream of the large Eurasian landmass and just north of Africa, European aerosols in particular have thus potential impact on huge inhabited areas, both through local impacts and through remote impacts mediated by atmospheric circulation adjustments. Their impact throughout the twentieth century, however, has not been consistently investigated so far in a multi-model framework, particularly for the earlier part of the century when aerosol effects might have been disproportionately large in a cleaner atmosphere (Carslaw et al., 2013). This is a gap this study aims to address. We make use of experiments carried out as part of the Coupled Model Intercomparison Project Phase 5 (CMIP5) initiative (Taylor et al., 2012). These comprise of multiple realizations of experiments of all historical forcings as well as individual forcings with a range of coupled global climate models, which allows us to analyze the effect of anthropogenic aerosol and compare it to those of other forcing factors, both when acting in isolation and when combined. The availability of a large set of simulations allows the identification of robust patterns of forced climate response

by (1) averaging over multiple members, thus reducing the effect of internal variability, and (2) sampling across various model formulations.

In order to provide a basic characterization of the climate response to NAEU aerosol emissions expected from CMIP5 simulations, we focus on the boreal summer season, when the aerosol impact on temperature and other variables mediated by temperature differences, such as the position of the ITCZ and the jet streams, is expected to be largest due to the insolation maximum in the northern hemisphere (see discussion in Hegerl et al. (1997)). The analysis examines changes in near-surface temperature (TAS), precipitation, diurnal temperature range (DTR), sea level pressure (SLP), and zonal wind at 300 hPa. This subset, although limited, allows us to identify the aerosol impact on relevant surface climate features, some of which are long-term observed, and investigate the potential of aerosols to bring about changes in the atmospheric circulation.

The remainder of the manuscript is organized as follows: After a short description of the datasets and the analysis methods used (Section 2), we illustrate the spatio-temporal changes in anthropogenic aerosol emissions and the resulting atmospheric aerosol loading and radiative effect (Section 3). The linear trends in the all-forcing and single-forcing CMIP5 ensembles during the historical period of increasing NAEU sulphate emissions are then shown, contrasted by those during the later period of decreasing NAEU emissions (Section 4). While this captures multi-decadal to near-centennial changes, higher-frequency variability of European near-surface temperature, sea level pressure, and DTR are analyzed by means of area-mean time series also from observations, and the contribution of each single-forcing factor to the total simulated forced inter-decadal variability is estimated (Section 5). The study is completed by summary and conclusions (Section 6).

2. Data and methods

We use data from the CMIP5 twentieth century historical experiments, and select models which provide simulations forced only with anthropogenic aerosols (Tab. 1). In addition to this ensemble of aerosol-only simulations ("AA"), we also analyze simulations with forcing from well-mixed greenhouse gases only ("GHG"), natural forcings only (solar radiation and volcanoes, "NAT"), and all these forcings combined ("ALLF") for the same set of models. Note that ALLF are the standard historical simulations, which are expected to reproduce the observations. For each model, we choose ensembles of GHG, NAT, and ALLF with the same size as the ensemble available for AA, so that the results from the different ensembles are comparable. Results from the trend analysis are shown for the multi-model mean ("MMM"), obtained by first averaging the individual ensemble members for each model and successively averaging these ensemble means. Given the different ensemble sizes -ranging from one to five- this ensures that each model is given equal weight.

While the chosen subset has a more comprehensive representation of aerosol effects compared to the full suite of CMIP5 models (Taylor et al., 2012), there is still substantial variation amongst the models (Ekman, 2014): In GFDL-CM3 and NorESM1-M, aerosol micro-physics and chemistry including cloud droplet number concentration (CDNC; first indirect effect) are simulated online, and precipitation formation depends on this CDNC (second indirect effect). CSIRO-Mk3.6.0, HadGEM2-ES, and CanESM2 also have online aerosols schemes, but use diagnostic CDNC formulations, on which precipitation does (CSIRO-Mk3.6.0, HadGEM2-ES) or does not (CanESM2) depend. GISS-E2-R and IPSL-CM5A-LR prescribe aerosol fields from offline calculations, use diagnostic CDNC representations, which precipitation does (GISS-E2-R) or does not

(IPSL-CM5A-LR) depend on. On top of these differences, the chemistry models used and/or the way of the diagnostic derivation of CDNC may vary as well.

Given that all models are forced with the same aerosol emission inventories (Lamarque et al., 2010), the use of multiple models does thus not only reduce the contribution from internal variability, but allows us moreover the identification of features which are robust to these differences in the models' representation of indirect aerosol effects as well as their aerosol distribution and background (pre-industrial) aerosol concentrations (Wilcox et al., 2015). This is important since these inter-model differences have been found to cause a large spread in the aerosol responses (Boucher et al., 2013; Kasoar et al., 2016)). Robustness is assessed by comparing the sign of the response in the MMM with that in the models' ensemble means.

The models considered span the full range of CMIP5 spread in climate sensitivity (Flato et al., 2013), and represent the diversity in the effective radiative forcing due to direct and indirect aerosol effects combined (Zelinka et al., 2014). Their historical all-forcing MMM reproduces the climatology and observed changes in surface temperature patterns, and simulates the climatology of many large-scale circulation features reasonably well (Flato et al., 2013; Kumar et al., 2016). For DTR, too, the all-forcing simulations from chosen CMIP5 models separately as well as the MMM of all models' all-forcing simulations agree well with observations over Europe both in terms of climatology (Lindvall and Svensson, 2014; Cattiaux et al., 2015; Liu et al., 2016) and long-term trends (Lewis and Karoly, 2013).

The aerosol forcing in all models is based on decadal aerosol emissions with an annual cycle. We compute boreal summer (June, July, and August, "JJA") means from monthly-mean data, and all model data is re-gridded prior to further analysis to match the model with the lowest resolution, which is 3.75°x2.8°. For the comparison with observations, we instead interpolate the model data to the observational resolution and mask according to the observational coverage. Anomalies

from the climatological state are considered, and the climatologies are computed from the models' pre-industrial control simulations.

Simulated temperature and sea-level pressure changes are compared to those derived from available observational data. For near-surface temperature anomalies, we use the HadCRUT dataset version 4.5 ("HadCRUT") (Morice et al., 2012), the CRUTS dataset Version 3.24.01 ("CRU") (Harris et al., 2014), the gridded Berkeley Earth Surface Temperature dataset ("BEST") (Rohde et al., 2013b), and GISS Surface Temperature Analysis ("GISTEMP") (GISTEMP Team, 2017; Hansen et al., 2010). For DTR, we use CRU and BEST, and for sea level pressure we use the Met Office Hadley Centre mean sea level pressure data set HadSLP2 (1850-2004, "HadSLP") (Allan and Ansell, 2006).

We compute DTR from the CMIP5 model data as the difference between monthly-mean Tmax and monthly-mean Tmin, as provided by the modelling groups (see Tab. 1), and follow the same procedure for the BEST dataset; for the CRU data, monthly-mean DTR is used as provided by Harris et al. (2014). Note that the observational datasets differ in their station input sources, time sampling, quality control, homogenization, and area-averaging; for a comprehensive analysis of the relevance of these differences see Thorne et al. (2016).

Long-term changes in climate are investigated by computing linear trends, calculated as least-squares regressions, and displayed as change per decade. The robustness of the simulated trends is measured by the agreement among the various models: Stippled areas are regions where at least all but one of the models' ensemble means (i.e. 5 out of 6 or 6 out of 7, depending on the availability of some variables for specific experiments) agree on sign. The time period common to all model simulations is 1860-2005, but we limit the analysis to 1900 onward when observations are less sparse (Morice et al., 2012). Trends in the NAT ensemble are not shown for brevity unless otherwise stated, as they are found to be small compared to those in the AA and GHG

ensembles as well as barely anywhere robust across models for the variables, time periods, and regions considered in this analysis.

In order to support the use of linear trends to identify the link between aerosol loading and near-surface temperature, a joint empirical orthogonal functions (EOF) analysis is also performed (Deser and Blackmon, 1993; Wang et al., 2016). This method, which is an ordinary EOF analysis of the two variable fields combined in space, decomposes the data into orthogonal modes each consisting of one pattern per variable and a common time series, ordered by the fraction of combined variance explained. In contrast to a regression analysis, this identifies covarying patterns without the need to presume timeseries or spatial patterns. Prior to the EOF analysis, the data are temporally smoothed in order to suppress inter-annual variability. This is done by taking subsequent 11- and 7-year running means which improves filter characteristics relative to taking running means only with a single window length (e.g. von Storch and Zwiers (1999)). For a sensitivity analysis see supplementary Text S1.

3. Spatio-temporal changes in aerosol emissions and associated near-surface temperature

Sulphur dioxide (SO2) is the main component of anthropogenic aerosol emissions (Lamarque et al., 2010; Hoesly et al., 2017). The time series of total SO2 emissions from various regions illustrate the dominance of NAEU emissions from pre-industrial times until the mid-twentieth century and show the peak in the 1970s, with the trend reversing in Europe around 1975, following a slightly earlier reversal in the US (Fig. 1). While Asian (incl. eastern Russian) emissions also started to increase before 1970, they do not exhibit strong (Japan, Russia) or any (China, India, etc.) downward trends afterwards. This is also visible in the spatial pattern of the linear trends of SO2 emissions during 1900-1970 and 1971-2010 (Fig. 2).

The corresponding trend patterns in column-integrated sulphate content (sulphate loading) and aerosol optical depth at 550 nm (AOD) in the CMIP5 model ensemble show that aerosols spread further east of the source region towards central Eurasia as a result of transport by the climatological westerlies (Fig. 2). Although CMIP5 models use the same aerosol emission inventories, the simulated aerosol distribution patterns may vary from model to model due to differences in meteorology, chemical parameterizations, and pre-industrial background concentrations (Carslaw et al., 2013; Wilcox et al., 2015; Kasoar et al., 2016). Nonetheless, there is considerable agreement on the sign of the trends over Eurasia (Fig. 2c-d). The emissions of other aerosol species (black carbon, organic carbon) changed over time less homogeneously in space (Figs. S1-4), but the simulated changes in AOD, which integrates the amount and optical properties of all simulated aerosol species, are very similar to those in sulphate loading, thus reflecting the dominance of sulphate aerosols (Fig. 2e-f).

A joint EOF analysis reveals modes of covariability of sulphate loading and near-surface temperature (TAS) as simulated in the AA ensemble for summer over the NH excluding the Pacific (Fig. 3). The dominant temperature signature is a large-scale cooling associated with an overall increase in sulphate aerosols until they peak in the 1970s (Fig. 3a). The first mode's patterns and time series for both sulphate loading and TAS are very similar to those of the first mode from EOFs of the variables separately (Fig. S5a-b), which confirms that these patterns represent a substantial part of variability in both sulphate loading and TAS individually in the CMIP5 ensemble. Separate EOF analyses of other variables show that approximating the aerosol-related impact with linear trends captures a large fraction of their variability in the CMIP5 AA ensemble (for example precipitation and DTR, Fig. S5c-d).

The higher modes from the joint EOF analysis reflect differences in the time series of aerosol emissions and associated temperature impacts at smaller spatial scales. The sulphate loading and

temperature patterns of the second mode (Fig. 3b), for instance, has opposite signs in North America and Europe compared to Asia. The principal components accordingly resemble the time series of the difference in sulphate loading over these regions. However, since only a very small fraction of the covariance is explained by the higher modes, we focus here on the dominant behavior as reflected in the first mode.

4. Simultaneous long-term changes in NAEU emissions and near-surface climate

Given the strong opposite trends in SO2 emissions from NAEU before and after the peak in the 1970s, it is reasonable to expect their climate signature to also show a trend reversal around the same time. Emissions from elsewhere, e.g. Asia, in contrast, started to increase in the 1950s and might thus have perturbed the climate during the first period, but we expect their continued increase during the second period to result in changes of the same sign in both periods, albeit of different magnitudes. This also holds true for GHG forcing, which has increased during both periods. We thus identify changes during 1900-1974 in the ALLF ensemble as dominantly driven by NAEU aerosol forcing if they are robust and have the same sign as those in the AA but different to those in the GHG or NAT ensembles. This approach is further validated by contrasting the trends with those during 1975-2005, when we expect the decreasing NAEU emissions to drive changes of the opposite sign. Note, however, that the impact of emissions from, say, Asia is not negligible during 1975-2005, so that the effect of decreasing NAEU emissions might be offset by Asian emissions.

Despite clear limitations, this approach allows us to disentangle the NAEU aerosol imprint in presence of other forcings (provided they changed monotonously during the whole record). The advantage over other methods (e.g., EOF analysis) is that it allows us to assess inter-model consistency and to compare with the other ensembles and observations, for which aerosol data are not available.

Based on the timing of the trend reversal in simulated sulphate loading (indicated by a black line in the time series in Fig. 3), we choose 1900-1974 and 1975-2005 as the time periods with increasing and decreasing aerosols, respectively. Note that choosing instead the partition year 1970, as done for the trends in emissions because they are decadal only, does not affect the results reported below (not shown). The first time period includes the slow increase in emissions (Fig. 1), so that trends per decade are smaller during the first than the second period; European area-mean (35-60°N, 0-60°E) trends in the aerosol-only MMM amount to +2.0 and -2.6 mg/m2/decade for sulphate loading and +0.028 and -0.046 1/decade for AOD during 1900-1975 and 1975-2005, respectively.

Because emissions from both North America and Europe reversed sign around this time, we will in the following attribute the changes to NAEU emissions. The larger trends in European emissions and their closer proximity to the area studied, however, might suggest them to have a larger share of the impacts at least on Eurasian near-surface temperature.

a. Near-surface temperature & sea level pressure

The CMIP5 AA ensemble shows a widespread decrease in near-surface temperature over the Atlantic-Eurasian region during the period of increasing NAEU emissions (Fig. 4a). This trend is reversed in the later period with a warming of similar magnitude as the earlier cooling over central Europe, and a slightly weaker warming over the Asian mid-latitudes (Fig. 4b). Note that over eastern China, temperatures decrease during both periods consistent with trends in local aerosol emissions (Fig. 2a,c), so NAEU emissions are not the (sole) driver of the cooling over this region in the CMIP5 models. The larger trends during the second period -shown in Fig. 4 scaled by a factor of one half- compared to those during the first period are consistent with the larger trends in emissions, sulphate loading, and AOD (Fig. 2).

GHG forcing produces warming during both periods (Fig. 4e-f), and both the AA and the GHG signature are robust across the models in the whole region. In the ALLF ensemble, which has the two anthropogenic forcings counteract each other in the first period, the models agree on the mid-latitude cooling as well as the warming at higher and lower latitudes. The zonally extended temperature anomalies are consistent with Shindell et al. (2010), who found the influence of inhomogeneous radiative forcing to extend three to four times further in the zonal than in the meridional direction. The vertical cross-section of temperature trends averaged over 30-60°N shows moreover that although the strongest cooling is located near the surface over Europe, the temperature signal extends up to the mid- and upper-troposphere and as far eastward as central Asia (Fig. S6a-b), suggestive of an eastward propagation from Europe. Natural forcing does not result in appreciable trends in the CMIP5 models (not shown).

Sea level pressure, consistent across the models, shows anomalous anticyclonic trends over the Eurasian mid-latitudes in the first period both in the AA and the ALLF ensemble, which is consistent with the atmospheric adjustment to the surface cooling (Figs. 4a,c; S7a,c). The largest aerosol-induced anomalies in TAS and SLP east of the area of highest emission changes (Figs. 4, S6-7) is consistent with expectations from aerosol transport as well as temperature advection by climatological westerlies (not shown). While increasing anthropogenic aerosols thus dominate the simulated Eurasian mid-latitude temperature changes during 1900-1974, simulated tropical temperature changes appear to be more strongly influenced by GHG forcing, with a widespread warming seen both in the GHG and the ALLF CMIP5 ensembles (Fig. 4c-f).

b. Jet stream strength and position

The zonal character of the aerosol-driven temperature changes as simulated with the CMIP5 models suggests that aerosols might also affect circulation features in the latitudinal direction

via changes in the meridional temperature gradients. We find indeed that both the AA and the ALLF ensemble show a strengthening of the equatorward side of the subtropical jet over Asia, as identified from changes in 300-hPa zonal wind strength, during the first time period, and a weakening during the second period (Fig. 5a-d). GHG (and NAT, not shown), on the other hand, show no large-scale significant or robust trends (Figs. 4e-f; 5e-f). This is consistent with the thermal wind relation, with AA cooling the mid-latitudes more than the tropics and thus enhancing the temperature gradient, which results in a strengthened zonal wind (Figs. 4a,c; 5a,c). Conversely, during the second period, the decrease in NAEU emissions warms the mid-latitudes more than the tropics, thus reducing the gradient and weakening the zonal wind (Figs. 4b,d; 5b,d). The significant positive wind speed anomalies on the southern flank of the climatological jet position during the first period, and negative ones during the second, can be additionally interpreted as a southward and northward, respectively, displacement of the circulation in response to the changing meridional temperature gradients.

c. Precipitation

Another feature associated with the change in the meridional circulation is the shift of the inter-tropical convergence zone (ITCZ) in response to variations in the inter-hemispheric temperature gradient, driven by the aerosols' preferential cooling of the Northern vs. the Southern hemisphere (Chiang and Friedman, 2012; Hwang et al., 2013). In the CMIP5 models, we also see an aerosol signal on precipitation over western Africa, where rainfall is largely controlled by the ITCZ (Undorf et al., 2018): A drying during the period of increasing NAEU aerosols, and a wettening during the period of decreasing aerosols, both in the AA and the ALLF ensemble (Fig. 6a-d).

Over most of Eurasia, where climatological precipitation is relatively low and spatially heterogeneous, precipitation trends in the CMIP5 AA ensemble during 1900-1974 are small (Fig. 6a).

Key robust features are a wettening trend over western Europe as well as a drying over the high-latitudes, including Scandinavia and Northern Russia, which is also reversed during 1975-2005 (Fig. 6b). The ALLF ensemble shows also that if aerosols are included, the drying over Europe as simulated for GHG forcing only is restricted to the Mediterranean (Fig. 6c-f).

In the subtropical and tropical monsoon regions South Asia, East Asia, western Africa, in contrast, we see a robust aerosol signal during both periods (Fig. 6a-d). During the first period, the AA ensemble shows a drying over northern India, which reverses during the second period (Fig. 6a-b). This robust and significant aerosol signal also dominates -although over a smaller domain- in the ALLF ensemble, despite the counteracting effect of GHGs (Fig. 6c-f).

Both the AA and the ALLF ensemble also show a meridional tripole pattern of longitudinally-elongated bands featuring a drying over central China and the western Pacific, a wettening over southern China and Indochina, and again a drying over the Maritime Continent during the first period (Fig. 6a,c). This pattern is especially consistent between AA and ALLF over land, whereas the GHG impact appears to emerge in driving the oceanic precipitation increase over the Indian Ocean and the western Pacific (Fig. 6e). While these precipitation changes have thus been clearly driven by anthropogenic aerosols in the CMIP5 models, our results do not allow us to unequivocally separate the role of remote and local aerosols, owing to the simplicity of the linear-trend approach: In addition to NAEU emissions, local emissions also increased -again potentially more effective than later in the century-, the effects of which presumingly added onto those from NAEU emissions (Guo et al., 2013). The importance of NAEU aerosols is clear, however, from comparison with a shorter, earlier period (1900-1950) for which the assumption of negligible Asian emissions change is even more justified (Fig. 1): The precipitation changes during 1900-1975 when both NAEU and Asian emissions increased strongly resemble those during 1900-1950, when only NAEU emissions increased, so that the response to NAEU forcing must be a substantial part of the response

to the combined forcing (Figs. 6, S10). Impact from NAEU aerosols in our results is plausible, too, since the anomalous anticyclone over mid-latitude Asia, resulting from the large-scale near-surface and tropospheric cooling (Figs. 4, S6-7) might cause northeasterly winds which oppose the climatological monsoon flow and thus induce a weakening of the East Asian summer monsoon circulation, as visible in the precipitation changes over East Asia (Figs. 6). During 1975-2005, on the other hand, the impact of increasing local emissions could have counteracted that of decreasing NAEU emissions (Guo et al., 2013), and the continued drying suggests that NAEU emissions were not the most important factor in driving the precipitation changes over China and South-East Asia in the CMIP5 simulations during this later period (Fig. 6a-b).

d. Diurnal temperature range

DTR shows a widespread decrease over much of the European and Asian mid-latitudes both in the AA and the ALLF ensemble during the first time period (Fig. 7a,c). Over Europe, the trend is reversed during the second period (Fig. 7b,d). The trends in the GHG ensemble (and NAT, not shown) are less uniform and not consistent with ALLF (Fig. 7e-f), which suggests that aerosols, not greenhouse gases, dominate the twentieth century DTR variations over Europe, in agreement with expectations. Interestingly, a significant, consistent aerosol signal is also noticeable at low latitudes (from northern Africa to India), but of opposite sign to that in the mid-latitudes, with GHG (and NAT) trends again much smaller, less robust, and inconsistent with those in the ALLF ensemble; coinciding precipitation trends (Fig. 6) hint at modulations in diurnal convection by changes in cloudiness as a possible mechanism underlying this aerosol control on DTR over these regions, which is supported by trends in total cloud fraction (Fig. S8).

e. Sensitivity study and early twentieth century

The robustness of the trends during 1900-1974 is further ascertained by considering the shorter 1900-1950 period, during which Asian emissions increased even less and were at levels comparable to those of combined European and North American emissions in 1850 (Fig. 1). During this period, trends of similar patterns to those for 1900-1974 emerge in the CMIP5 simulations over the region considered, but with smaller magnitudes, as expected from the smaller increase in aerosols (and GHGs) which had taken place by then (Figs. S9-11). For near-surface temperature, the cooling in the AA ensemble during 1900-1950 does not dominate the ALLF response, but reduces the warming trends over Europe seen in the GHG ensemble in the mid-latitude band which shows aerosol-related cooling during 1900-1974. The pattern of change in precipitation over South-East Asia described above is already recognizable in the AA trends during 1900-1950; also, DTR shows a robust narrowing over the mid-latitudes in both the AA and the ALLF ensemble.

These findings suggest that aerosols were already a key driver of regional climate anomalies before the peak aerosol increase between 1950-1970s, for some variables even dominant over GHGs. Note that saturation effects might contribute to this by potentially making the aerosol emissions less effective later in the twentieth century (e.g. Carslaw et al. (2013)). The similarity of the patterns and their already considerable magnitude during 1900-1950 furthermore support the notion that remote (NAEU) emissions contributed substantially to the simulated near-surface climate variation over Russia and Asia, since the amount of remote aerosol emissions dominated over that of local emissions even more in 1950 than in 1970: In 1950 (1970), there were 8 (4) times more emissions from Europe than from Asia, and from 1900-1950 (1900-1970), those from Europe increased nearly 6 (3) times faster than those from Asia (Fig. 1).

5. Temporal evolution of European climate

a. Comparison with observations

In this section, the model-based findings on long-term changes associated with aerosols discussed above are complemented by an analysis of area-mean time series for the region with the largest trends in the AA and ALLF ensembles (35°-60°N, 0°-60°E) (Fig. 8). We focus on near-surface temperature, sea-level pressure, and DTR, which all show a spatially homogeneous response across this region in the CMIP5 ensemble (Fig. 4,7). These time series are also compared with observations, the coverage of which is better for this region than most others especially early in the twentieth century.

The temporal change in near-surface temperature shows the contrast between the warming in the GHG-only experiments and the cooling in the AA ensemble (Fig. 8a). The small gradients in both ensembles in the first decades of the twentieth century is consistent with weak variations in anthropogenic emissions, while clear differences between the gradients in the two ensembles start appearing around 1925, with similar magnitudes of opposite sign until the 1970s. The largest aerosol-induced variations are found during 1940-1975, followed by a plateau and a weak recovery, reflecting the peak and subsequent decline in global aerosol emissions. In contrast, the GHG warming increased exponentially during the twentieth century, with the largest trends after 1960. The all-forcing ensemble reflects the modulation due to both drivers as well as the contribution from natural variability, for example the volcanic cooling (e.g. after the Agung eruption in 1963, e.g. Robock and Mao (1995)). After a few decades of negligible anthropogenic forcing at the beginning of the century, temperature variations are dominated by aerosol cooling until at least 1970, when GHG warming starts to dominate instead. Comparison with the observed changes shows that the CMIP5 models are able to capture the observed twentieth century variations of near-surface

temperature over Europe (observations within the 95% range of ALLF). The most notable feature in the observations is the cooling during 1940-1980, which is consistent with the prevailing role of anthropogenic aerosols.

For sea level pressure (Fig. 8b) and DTR (Fig. 8c), the single-forcing ensembles diverge less clearly, reflecting higher variability, lesser model agreement, and more complex responses of these variables compared to temperature to the different forcings. For SLP, both the AA and the ALLF ensemble encompass the observations, but the GHG and NAT ensembles do not, indicating that aerosol forcing is essential to explain the observed variations.

For DTR, the two observed datasets agree on multi-decadal variability, showing a decrease until 1930, followed by a steep increase, and a subsequent decrease between the mid-1930s and the mid-1980s. They differ in their absolute anomalies, however, due to discrepancies in the first half of the century (Thorne et al., 2016). While all ensembles are compatible with the CRU observations at the 95% level, the GHG and NAT ensembles are incompatible with the BEST dataset in the second half of the twentieth century. The AA and ALLF ensembles are the only ones to show a DTR narrowing over most of the twentieth century as do the observations. This overall provides further confirmation of aerosol forcing being necessary to explain historical observed variations. However, due to strong influence of internal climate variability, conclusive attribution of observed changes was not possible.

b. Contribution of individual forcings to simulated European summer climate

The contribution of each single forcing on the forced component of simulated European inter-decadal climate variability can be estimated by calculating the gradient of the multi-model mean time series from each ensemble and comparing the magnitude of those from the single-forcing CMIP5 ensembles (AA, GHG, NAT) to their arithmetic sum as in Wilcox et al. (2013). This

approach assumes that the role of internal variability is negligible in the multi-model mean and that the responses to the individual forcings add linearly (Fig. 9). The time series are smoothed prior to the analysis by consecutively taking 11- and 7-year running means to suppress variability on time scales shorter than inter-decadal (Section 2).

For European near-surface temperature, the sum of the gradients (AA+GHG+NAT) is a reasonable approximation to the gradient from the ALLF ensemble (Fig. 9a, top), and during the twentieth century, the contribution of AA to the total forced simulated variability (36%) is comparable to that of GHG (43%), and larger than that of NAT (21%). The aerosol impact is even dominant during 1940-1970, with AA explaining more than 50% of the total forced variability. The aerosol contribution to the total forced inter-decadal model variability in sea level pressure is also discernible and amounts to about a third throughout the twentieth century, and slightly more again in the period 1940-1970 (Fig. 9b). For DTR, AA contributes on average a forth throughout the twentieth century; this contribution grows towards the later decades, but then the sum of the gradients of the single-forcing time series approximates the all-forcing one less well (Fig. 9c).

6. Summary, discussion, and conclusions

The long-term signature of anthropogenic aerosol emissions mainly from North America and Europe (NAEU) on Eurasian summer climate throughout the twentieth century has been identified in an ensemble of coupled climate (CMIP5) models. The analysis was motivated by the need to advance current understanding of the effects of aerosols on regional climate, which is of utmost importance to more confidently assess and quantify the drivers of past climate variations as well as to reduce uncertainties in near-future climate projections. North America and Europe were the key aerosol emission regions worldwide for most of the twentieth century, with the potential to influence climate downstream over large inhabited regions. Yet, the topic has not been consistently

investigated so far: While earlier studies have mostly focused either on individual variables or used only one climate model, robust information on the aerosol impact on a range of relevant variables across multiple coupled models is still largely unknown.

The aerosol imprint on simulated summer climate was inferred from inter-model agreement on linear trends during a period of increasing NAEU sulphate emissions (1900-1974), contrasted with trends during the more recent period of decreasing emissions (1975-2005). This was supported by an analysis of the covariability of near-surface temperature and sulphate loading. The main findings are:

- Regionally and during the 1900-1974 period, aerosols generated a large-scale anomalous cooling stretching from Europe across most of the Eurasian mid-latitudes in the CMIP5 models. The cooling, largest at the surface, extends to the mid and upper troposphere, and is associated with a large-scale anticyclonic sea-level pressure anomaly centered over Russia, as well as with a widespread narrowing of DTR. Aerosols also strengthened the northern hemisphere subtropical jet on its equatorward side, which is consistent with changes in the meridional temperature gradient, and decreased monsoon precipitation over western Africa, northern India, and eastern China.

- During the 1975-2005 period, most of these changes are reversed, which provides support to their association with NAEU sulphate aerosol emissions – only precipitation changes over East Asia, where strong positive trends in local aerosol emissions are expected to superpose the effect of decreasing NAEU emissions, do not reverse.

- Analysis of observations averaged across Europe shows clear evidence for aerosols and GHGs both being important for models to reproduce inter- and multi-decadal variations in near-surface temperature. Observed variations in sea-level pressure are noisy, but tend to agree

much better with simulations that include anthropogenic aerosols than with those without aerosols. Observed DTR has very high data uncertainty, but shows a decline over much of the century that does not occur in the CMIP5 GHG and NAT ensembles.

- Assuming linearity among the single forcing responses, anthropogenic aerosols are estimated to explain on average more than a third of the forced simulated inter-decadal variability in European near-surface temperature during the twentieth century, and more than half during 1940-1970.

The time-series analysis thus highlights the importance of aerosols in addition to GHGs for explaining temporal variations in observed European near-surface climate, in agreement with Bindoff et al. (2013). For DTR, our results add onto those by Makowski et al. (2008), providing the evidence from an ensemble of CMIP5 experiments. Furthermore, we show that regionally AA explain a substantial fraction of simulated European climate inter-decadal variability from as early on as 1900, which is even larger than that found by Wilcox et al. (2013) for global mean temperature.

Significant changes in strength and latitudinal position of the subtropical jet stream during the twentieth century have been discussed in a number of studies, including those focusing on variations of the tropical belt width, given that the jet stream can be interpreted as the poleward boundary of the tropics. While some studies only looked at annual means (Archer and Caldeira, 2008b; Fu and Lin, 2011; Moore, 2013) or the winter season (Strong and Davis, 2007), changes in winter and summer, if any, were generally found to be consistent in sign (Archer and Caldeira, 2008a; Hudson, 2012; Davis and Birner, 2013; Pena-Ortiz et al., 2013; Abish et al., 2015), despite the pronounced climatological seasonality. Evidence suggests a weakening and/or poleward shift of the NH subtropical jet since 1979 from satellite observations (Fu and Lin, 2011), reanalyses (Archer and Caldeira, 2008a; Hudson, 2012), and observations (Davis and Birner, 2013; Pena-Ortiz et al.,

2013). Together with weaker and/or even opposite trends since the mid-twentieth century (Strong and Davis, 2007; Archer and Caldeira, 2008b; Pena-Ortiz et al., 2013; Abish et al., 2015) and ice core proxy data (Moore, 2013), this indicates a strengthening before 1979. In the framework of tropical expansion/contraction, these changes have been previously linked to sulphate forcing (Allen et al., 2012, 2014; Allen and Ajoku, 2016; Ming et al., 2011), especially during the summer (Tao et al., 2016), but the sign reversal associated with the evolution of aerosol forcing throughout the 20th century has not been previously discussed in the context of jet stream changes, and the appearance of noticeable trends as early as the beginning of the century has not been shown yet.

The remote impact on monsoon precipitation found here in the CMIP5 models is consistent with Polson et al. (2014). For western Africa, observations show similarly a drying during 1950-1985, and a recovery thereafter (Nicholson, 2013), and the region has been identified as sensitive to aerosol forcing (e.g. Rotstayn and Lohmann (2002); Ackerley et al. (2011)). Dong et al. (2014), who found both Asian and European sulphur dioxide emissions relevant for the decreased West African precipitation, and Undorf et al. (2018), who attributed observed precipitation changes over West Africa during 1920-2005 mainly to NAEU emissions, both used a single model. Our results, based on a range of CMIP5 models, also indicate the predominant importance of NAEU emissions on summer monsoon precipitation over western Africa. The overall weakening of the South Asian monsoon during the second half of the twentieth century forced by anthropogenic aerosols has been acknowledged before (e.g. Bollasina et al. (2011)). While other studies found regional and remote aerosols responsible in varying ratios (e.g. Bollasina et al. (2014); Guo et al. (2015)), we show that considering the periods with increasing and decreasing remote emissions separately indicates remote emissions to be most important. For East Asia, we found remote emissions not dominant during 1975-2005, consistent with strong impact of local aerosols (e.g. Guo et al. (2013)), but our results do not exclude substantial impact of remote aerosols, especially

before 1975, and are not inconsistent with a mechanism of remote aerosol impact on monsoon precipitation found in earlier studies (Cowan and Cai, 2011; Dong et al., 2015).

The models used in this study explore the range of climate sensitivity and aerosol forcing of those CMIP5 models that include a representation of indirect effects, from those with weak (e.g. IPSL-CM5A-LR) to those with strong (e.g GFDL-CM3) indirect effects (Section 2). Previous studies, however, showed substantial differences between the response to historical aerosol emissions in CMIP5 models with and without a representation of aerosol indirect effects (Wilcox et al., 2013; Guo et al., 2015); other models, which neglect indirect aerosol effects, might therefore misrepresent the response to aerosol emissions as identified in this study.

While the use of historical single- and all-forcing simulations allows us to identify features of aerosol impact within the system of interactions and feedbacks -insofar represented in the models-, targeted simulations would allow a more rigorous disentanglement of the effects of aerosols from different source regions, including NA and EU. Similarly, the CMIP5 models' differing aerosol representations increase the robustness of our findings, but also prevent us from exploring the mechanisms of aerosol impact further. A future study with a different focus would thus complement our work and help understand better the physical mechanisms mediating NAEU aerosol impact.

To conclude, the findings add valuable information about the robustness of the aerosol impacts as well as new insights on their climate footprint, such as their modulation of DTR and the jet stream. The symmetry of the simulated impacts during the period of increasing and of decreasing emissions also sheds light on the changes to be expected from future reductions in aerosol emissions from NAEU and elsewhere.

Acknowledgments. We thank Laura Wilcox for discussion and data. The authors acknowledge the use of observational data from the Met Office Hadley Centre, the Climatic Research Unit at the University of East Anglia, Berkeley Earth, and the NASA Goddard Institute for Space Studies. We also thank the World Climate Research Program's Working Group on Coupled Modeling, the climate modeling groups (Tab. 1), the U.S. Department of Energy's Program for Climate Model Diagnosis and Inter-comparison and the Global Organization for Earth System Science Portals. This work was supported by the ERC funded project (EC-320691) TITAN. G. Hegerl is funded by NCAS and the Wolfson Foundation and the Royal Society as Royal Society Wolfson Research Merit Award holder (WM130060).

References

Abish, B., P. V. Joseph, and O. M. Johannessen, 2015: Climate Change in the Subtropical Jetstream during 1950 2009. *Adv. Atmos. Sci.*, **32**, 140–148, doi:10.1007/s00376-014-4156-6.1.

Ackerley, D., B. B. B. Booth, S. H. E. Knight, E. J. Highwood, D. J. Frame, M. R. Allen, and D. P. Rowell, 2011: Sensitivity of Twentieth-Century Sahel Rainfall to Sulfate Aerosol and CO 2 Forcing. *J Clim.*, **24**, 4999–5014, doi:10.1175/JCLI-D-11-00019.1.

Albrecht, B. A., 1989: Aerosols, Cloud Microphysics, and Fractional Cloudiness. *Science*, **245**, 1227–1230, doi:10.1126/science.245.4923.1227.

Allan, R., and T. Ansell, 2006: A new globally complete monthly historical gridded mean sea level pressure dataset (HadSLP2): 1850-2004. *J. Clim.*, **19 (22)**, 5816–5842, doi:10.1175/JCLI3937.1.

Allen, R. J., and O. Ajoku, 2016: Future aerosol reductions and widening of the northern tropical belt. *J. Geophys. Res. Atmos.*, **121 (12)**, 6765–6786, doi:10.1002/2016JD024803.

Allen, R. J., J. R. Norris, and M. Kovilakam, 2014: Influence of anthropogenic aerosols and the Pacific Decadal Oscillation on tropical belt width. *Nat. Geosci.*, **7**, 270–274, doi:10.1038/NGEO2091.

Allen, R. J., S. C. Sherwood, J. R. Norris, and C. S. Zender, 2012: Recent Northern Hemisphere tropical expansion primarily driven by black carbon and tropospheric ozone. *Nature*, **485 (7398)**, 350–354, doi:10.1038/nature11097.

Archer, C. L., and K. Caldeira, 2008a: Historical trends in the jet streams. *Geophys. Res. Lett.*, **35 (L08803)**, 1–6, doi:10.1029/2008GL033614.

Archer, C. L., and K. Caldeira, 2008b: Reply to comment by Courtenay Strong and Robert E. Davis on "Historical trends in the jet streams". *Geophys. Res. Lett.*, **35 (L24807)**, 1, doi:10.1029/2008GL035114.

Bindoff, N. L., P. A. Stott, M. AchutaRao, M. R. Allen, N. Gillett, D. Gutzler, K. Hansingo, G. Hegerl, Y. Hu, S. Jain, I. I.Mokhov, J. Overland, J. Perlwitz, R. Sebbari, and X. Zhang, 2013: Detection and Attribution of Climate Change: from Global to Regional. *Climate Change 2013: The Physical Science Basis. Contribution of Working Group I to the Fifth Assessment Report of the Intergovernmental Panel on Climate Change*, T. F. Stocker, D. Qin, G.-K. Plattner, M. Tignor, S. K. Allen, J. Boschung, A. Nauels, Y. Xia, V. Bex, and P. M. Midgley, Eds., Cambridge University Press, Cambridge, United Kingdom and New York, NY, USA.

Bollasina, M. A., Y. Ming, and V. Ramaswamy, 2011: Anthropogenic Aerosols and the Weakening of the South Asian Summer Monsoon. *Science*, **334 (6055)**, 502–505, doi:10.1126/science.1204994.

Bollasina, M. A., Y. Ming, and V. Ramaswamy, 2013: Earlier onset of the Indian monsoon in the late twentieth century: The role of anthropogenic aerosols. *Geophys. Res. Lett.*, **40 (14)**, 3715–3720, doi:10.1002/grl.50719.

Bollasina, M. A., Y. Ming, V. Ramaswamy, M. D. Schwarzkopf, and V. Naik, 2014: Contribution of local and remote anthropogenic aerosols to the twentieth century weakening of the South Asian Monsoon. *Geophys. Res. Lett.*, **41**, 680–687, doi:10.1002/2013GL058183.

Booth, B. B. B., N. J. Dunstone, P. R. Halloran, T. Andrews, and N. Bellouin, 2012: Aerosols implicated as a prime driver of twentieth-century North Atlantic climate variability. *Nature*, **484 (7393)**, 228–232, doi:10.1038/nature10946.

Boucher, O., D. Randall, P. Artaxo, C. Bretherton, G. Feingold, P. Forster, V.-M. Kerminen, Y. Kondo, H. Liao, U. Lohmann, P. Rasch, S. K. Satheesh, S. Sherwood, B. Stevens, and X. Y. Zhang, 2013: Clouds and Aerosols. *Climate Change 2013: The Physical Science Basis. Contribution of Working Group I to the Fifth Assessment Report of the Intergovernmental Panel on Climate Change*, T. F. Stockers, D. Qin, G.-K. Plattner, M. Tignor, S. K. Allen, J. Boschung, A. Nauels, Y. Xia, V. Bex, and P. M. Midgley, Eds., Cambridge University Press, Cambridge, United Kingdom and New York, NY, USA.

Branstator, G., 2002: Circumglobal teleconnections, the jet stream waveguide, and the North Atlantic Oscillation. *J. Clim.*, **15 (14)**, 1893–1910, doi:10.1175/1520-0442(2002)015⟨1893:CTTJSW⟩2.0.CO;2.

Carslaw, K. S., L. A. Lee, C. L. Reddington, K. J. Pringle, A. Rap, P. M. Forster, G. W. Mann, D. V. Spracklen, M. T. Woodhouse, L. A. Regayre, and J. R. Pierce, 2013: Large contribution of natural aerosols to uncertainty in indirect forcing. *Nature*, **503 (7474)**, 67–71, doi:10.1038/nature12674.

Cattiaux, J., H. Douville, R. Schoetter, S. Parey, and P. Yiou, 2015: Projected increase in diurnal and interdiurnal variations of European summer temperatures. *Geophys. Res. Lett.*, **42 (3)**, 899–907, doi:10.1002/2014GL062531.

Charlson, R. J., S. E. Schwartz, J. M. Hales, R. D. Cess, J. A. Coakley, Jr, J. E. Hansen, and D. J. Hofmann, 1992: Climate Forcing by Anthropogenic Aerosols. *Science*, **255**, 423–430, doi:10.1126/science.255.5043.423.

Chiacchio, M., T. Ewen, M. Wild, M. Chin, and T. Diehl, 2011: Decadal variability of aerosol optical depth in Europe and its relationship to the temporal shift of the North Atlantic Oscillation in the realm of dimming and brightening. *J. Geophys. Res. Atmos.*, **116 (2)**, 1–13, doi:10.1029/2010JD014471.

Chiang, J. C. H., and A. R. Friedman, 2012: Extratropical Cooling, Interhemispheric Thermal Gradients, and Tropical Climate Change. *Annu. Rev. Earth Planet. Sci.*, **40 (1)**, 383–412, doi:10.1146/annurev-earth-042711-105545.

Collins, W. J., N. Bellouin, M. Doutriaux-Boucher, N. Gedney, P. Halloran, T. Hinton, J. Hughes, C. D. Jones, M. Joshi, S. Liddicoat, F. O'Connor, J. Rae, C. Senior, S. Sitch, I. Totterdell, A. Wiltshire, and S. Woodward (2011), Model Development Development and evaluation of an Earth-System model - HadGEM2, *Geosci. Model Dev.*, *4*, 1051–1075, doi:10.5194/gmd-4-1051-2011.

Cowan, T., and W. Cai, 2011: The impact of Asian and non-Asian anthropogenic aerosols on 20th century Asian summer monsoon. *Geophys. Res. Lett.*, **38**, L11 703, doi:10.1029/2011GL047268.

669 Davis, N. A., and T. Birner, 2013: Seasonal to multidecadal variability of the width of the tropical
670 belt. *J. Geophys. Res. Atmos.*, **118 (14)**, 7773–7787, doi:10.1002/jgrd.50610.

671 Deser, C., and M. L. Blackmon (1993), Surface Climate Variations over the North Atlantic Ocean
672 during Winter: 1900-1989, *Journal of Climate*, *6*, 1743–1753.

673 Dong, B., R. T. Sutton, E. Highwood, and L. Wilcox, 2014: The Impacts of European and Asian
674 Anthropogenic Sulfur Dioxide Emissions on Sahel Rainfall. *J. Clim.*, **27 (18)**, 7000–7017, doi:
675 10.1175/JCLI-D-13-00769.1.

676 Dong, B., R. T. Sutton, E. J. Highwood, and L. J. Wilcox, 2015: Preferred response of the East
677 Asian summer monsoon to local and non-local anthropogenic sulphur dioxide emissions. *Clim.*
678 *Dyn.*, **46 (5)**, 1733–1751, doi:10.1007/s00382-015-2671-5.

679 Donner, L. J., B. L. Wyman, R. S. Hemler, L. W. Horowitz, Y. Ming, M. Zhao, J.-C. Golaz,
680 P. Ginoux, S.-J. Lin, M. D. Schwarzkopf, J. Austin, G. Alaka, W. F. Cooke, T. L. Delworth,
681 S. M. Freidenreich, C. T. Gordon, S. M. Griffies, I. M. Held, W. J. Hurlin, S. A. Klein, T. R.
682 Knutson, A. R. Langenhorst, H.-C. Lee, Y. Lin, B. I. Magi, S. L. Malyshev, P. C. D. Milly,
683 V. Naik, M. J. Nath, R. Pincus, J. J. Ploshay, V. Ramaswamy, C. J. Seman, E. Shevliakova,
684 J. J. Sirutis, W. F. Stern, R. J. Stouffer, R. J. Wilson, M. Winton, A. T. Wittenberg, and F. Zeng
685 (2011), The Dynamical Core, Physical Parameterizations, and Basic Simulation Characteristics
686 of the Atmospheric Component AM3 of the GFDL Global Coupled Model CM3, *J. Clim.*, pp.
687 3484–3519, doi:10.1175/2011JCLI3955.1.

688 Dufresne, J.-L., M.-A. Foujols, S. Denvil, A. Caubel, O. Marti, O. Aumont, Y. Balkanski, S. Bekki,
689 H. Bellenger, R. Benshila, S. Bony, L. Bopp, P. Braconnot, P. Brockmann, P. Cadule, F. Cheruy,
690 F. Codron, A. Cozic, D. Cugnet, N. de Noblet, J.-P. Duvel, C. Ethé, L. Fairhead, T. Fichefet,

S. Flavoni, P. Friedlingstein, J.-Y. Grandpeix, L. Guez, E. Guilyardi, D. Hauglustaine, F. Hourdin, A. Idelkadi, J. Ghattas, S. Joussaume, M. Kageyama, G. Krinner, S. Labetoulle, A. Lahellec, M.-P. Lefebvre, F. Lefevre, C. Levy, Z. X. Li, J. Lloyd, F. Lott, G. Madec, M. Mancip, M. Marchand, S. Masson, Y. Meurdesoif, J. Mignot, I. Musat, S. Parouty, J. Polcher, C. Rio, M. Schulz, D. Swingedouw, S. Szopa, C. Talandier, P. Terray, N. Viovy, and N. Vuichard (2013), Climate change projections using the IPSL-CM5 Earth System Model: from CMIP3 to CMIP5, *Clim Dyn*, *40*, 2123–2165, doi:10.1007/s00382-012-1636-1.

Dunstone, N. J., D. M. Smith, B. B. B. Booth, L. Hermanson, and R. Eade, 2013: Anthropogenic aerosol forcing of Atlantic tropical storms. *Nat. Geosci.*, **6**, 534–539, doi:10.1038/ngeo1854.

Ekman, A. M. L. (2014), Do sophisticated parameterizations of aerosolcloud interactions in CMIP5 models improve the representation of recent observed temperature trends?, *Journal of Geophysical Research: Atmospheres*, *119*, 817–832, doi:10.1002/2013JD020511.Received.

Flato, G., J. Marotzke, B. Abiodun, P. Braconnot, S. C. Chou, W. Collins, P. Cox, F. Driouech, S. Emori, V. Eyring, C. Forest, P. Gleckler, E. Guilyardi, C. Jakob, V. Kattsov, C. Reason, and M. Rummukainen, 2013: Evaluation of Climate Models. *Climate Change 2013: The Physical Science Basis. Contribution of Working Group I to the Fifth Assessment Report of the Intergovernmental Panel on Climate Change*, T. Stocker, D. Qin, G.-K. Plattner, M. Tignor, S. Allen, J. Boschung, A. Nauels, Y. Xia, V. Bex, and P. M. Midgley, Eds., Cambridge, United Kingdom and New York, NY, USA.

Folland, C. K., J. Knight, H. W. Linderholm, D. Fereday, S. Ineson, and J. W. Hurrel, 2009: The summer North Atlantic oscillation: Past, present, and future. *J. Clim.*, **22 (5)**, 1082–1103, doi:10.1175/2008JCLI2459.1.

713 Fu, Q., and P. Lin, 2011: Poleward shift of subtropical jets inferred from satellite-observed lower-
714 stratospheric temperatures. *J. Clim.*, **24 (21)**, 5597–5603, doi:10.1175/JCLI-D-11-00027.1.

715 Gillett, N. P., J. C. Fyfe, and D. E. Parker, 2013: Attribution of observed sea level pressure trends
716 to greenhouse gas, aerosol, and ozone changes. *Geophys Res Lett*, **40**, 2302–2306, doi:10.1002/
717 grl.50500.

718 GISTEMP Team, 2017: GISS Surface Temperature Analysis (GISTEMP), NASA Goddard Insti-
719 tute for Space Studies. Dataset accessed 2017-01-17 at URL https://data.giss.nasa.gov/gistemp/.

720 Guo, L., E. J. Highwood, L. C. Shaffrey, and a. G. Turner, 2013: The effect of regional changes
721 in anthropogenic aerosols on rainfall of the East Asian Summer Monsoon. *Atmos. Chem. Phys.*,
722 **13 (3)**, 1521–1534, doi:10.5194/acp-13-1521-2013.

723 Guo, L., A. G. Turner, and E. J. Highwood, 2015: Impacts of 20th century aerosol emissions on
724 the South Asian monsoon in the CMIP5 models. *Atmos. Chem. Phys.*, **15**, 6 367–6 378, doi:
725 10.5194/acp-15-6367-2015.

726 Hansen, J., R. Ruedy, M. Sato, and K. Lo, 2010: Global surface temperature change. *Rev. Geo-*
727 *phys.*, **48 (RG4004)**, 1–29, doi:10.1029/2010RG000345.

728 Hansen, J., M. Sato, and R. Ruedy, 1997: Radiative forcing and climate response. *J. Geophys.*
729 *Res.*, **102 (D6)**, 6831–6864, doi:10.1029/96JD03436.

730 Harnik, N., G. Messori, R. Caballero, and S. B. Feldstein, 2016: The Circumglobal North Amer-
731 ican wave pattern and its relation to cold events in eastern North America. *Geophys. Res. Lett.*,
732 **43 (20)**, 11,015–11,023, doi:10.1002/2016GL070760.

733 Harris, I., P. D. Jones, T. J. Osborn, and D. H. Lister, 2014: Updated high-resolution grids of
734 monthly climatic observations - the CRU TS3.10 Dataset. *Int. J. Clim.*, **34 (3)**, 623–642, doi:
735 10.1002/joc.3711.

736 Hegerl, G. C., K. Hasselmann, U. Cubasch, J. F. B. Mitchell, E. Roeckner, R. Voss, and
737 J. Waszkewitz, 1997: Multi-fingerprint direction and attribution analysis of greenhouse gas,
738 greenhouse gas-plus-aerosol and solar forced climate change. *Clim Dyn*, **13**, 613–634, doi:
739 10.1007/s003820050209.

740 Hoesly, R. M., S. J Smith, L. Feng, Z. Klimont, G. Janssens-Maenhout, T. Pitkanen, J. J. Seibert,
741 L. Vu, R. J. Andres, R. M. Bolt, T. C. Bond, L. Dawidowski, N. Kholod, J.-I. Kurokawa, M. Li,
742 L. Liu, Z. Lu, M. C. P. Moura, P. R. O'Rourke, and Q. Zhang, 2017: Historical (1750 2014)
743 anthropogenic emissions of reactive gases and aerosols from the Community Emission Data
744 System (CEDS). *Geosci. Model Dev. Discuss.*, **(March)**, 1–41, doi:10.5194/gmd-2017-43.

745 Hudson, R. D., 2012: Measurements of the movement of the jet streams at mid-latitudes, in the
746 Northern and Southern Hemispheres, 1979 to 2010. *Atmos. Chem. Phys.*, **12 (16)**, 7797–7808,
747 doi:10.5194/acp-12-7797-2012.

748 Hwang, Y.-T., D. M. W. Frierson, and S. M. Kang, 2013: Anthropogenic sulfate aerosol and the
749 southward shift of tropical precipitation in the late 20th century. *Geophys. Res. Lett.*, **40 (11)**,
750 2845–2850, doi:10.1002/grl.50502.

751 IPCC, 2013: Climate Change 2013: The Physical Science Basis. Contribution of Working Group
752 I to the Fifth Assessment Report of the Intergovernmental Panel on Climate Change, Solomon,
753 S., D. Qin, M. Manning, Z. Chen, M. Marquis, K. B. Averyt, M. Tignor, and H. L. Miller, Eds.,
754 Cambridge University Press, Cambridge, United Kingdom and New York, NY, USA, 1535 pp.

Iversen, T., M. Bentsen, I. Bethke, J. B. Debernard, A. Kirkevåg, Ø. Seland, H. Drange, J. E. Kristjansson, I. Medhaug, M. Sand, and I. A. Seierstad (2013), The Norwegian Earth System Model, NorESM1-M - Part 2: Climate response and scenario projections, *Geosci. Model Dev.*, *6*, 389–415, doi:10.5194/gmd-6-389-2013.

Jeffrey, S., L. Rotstayn, M. Collier, S. Dravitzki, C. Hamalainen, C. Moeseneder, K. Wong, and J. Syktus (2013), Australia's CMIP5 submission using the CSIRO-Mk3.6 model, *Austr. Meteorol. Oceanogr. J.*, *63*, 1–13.

Kasoar, M., A. Voulgarakis, J.-F. Lamarque, D. T. Shindell, N. Bellouin, W. J. Collins, G. Faluvegi, and K. Tsigaridis (2016), Regional and global temperature response to anthropogenic SO2 emissions from China in three climate models, *Atmos. Chem. Phys.*, *16*(2009), 9785–9804, doi:10.5194/acp-16-9785-2016.

Kim, J., J. Shin, Y.-H. Lim, Y. Honda, M. Hashizume, Y. L. Guo, H. Kan, S. Yi, and H. Kim, 2016: Comprehensive approach to understand the association between diurnal temperature range and mortality in East Asia. *Sci. Total Environ.*, **539**, 313–21, doi:10.1016/j.scitotenv.2015.08.134.

Koffi, B., F. Dentener, G. Janssens-Maenhout, D. Guizzardi, M. Crippa, T. Diehl, S. Galmarini, and E. Solazzo, 2016: Hemispheric Transport Air Pollution (HTAP): Specification of the HTAP2 experiments Ensuring harmonized modelling. Tech. rep., Joint Research Centre (JRC), Luxembourg. doi:10.2788/725244.

Kumar, S., J. L. Kinter, Z. Pan, and J. Sheffield, 2016: Twentieth century temperature trends in CMIP3, CMIP5, and CESM-LE climate simulations: Spatial-temporal uncertainties, differences, and their potential sources. *J. Geophys. Res. Atmos.*, **121 (16)**, 9561–9575, doi:10.1002/2015JD024382.

Lamarque, J.-F., T. C. Bond, V. Eyring, C. Granier, A. Heil, Z. Klimont, D. Lee, C. Liousse, A. Mieville, B. Owen, M. G. Schultz, D. Shindell, S. J. Smith, E. Stehfest, J. Van Aardenne, O. R. Cooper, M. Kainuma, N. Mahowald, J. R. McConnell, V. Naik, K. Riahi, and D. P. van Vuuren, 2010: Historical (1850-2000) gridded anthropogenic and biomass burning emissions of reactive gases and aerosols: methodology and application. *Atmos Chem Phys*, **10 (15)**, 7017–7039, doi:10.5194/acp-10-7017-2010.

Lewinschal, A., A. M. L. Ekman, and H. Körnich, 2013: The role of precipitation in aerosol-induced changes in northern hemisphere wintertime stationary waves. *Clim. Dyn.*, **41**, 647–661, doi:10.1007/s00382-012-1622-7.

Lewis, S. C., and D. J. Karoly, 2013: Evaluation of historical diurnal temperature range trends in CMIP5 models. *J. Clim.*, **26 (22)**, 9077–9089, doi:10.1175/JCLI-D-13-00032.1.

Li, Z., W. K.-M. Lau, V. Ramanathan, G. Wu, Y. Ding, M. G. Manoj, J. Liu, Y. Qian, J. Li, T. Zhou, J. Fan, D. Rosenfeld, Y. Ming, Y. Wang, J. Huang, B. Wang, X. Xu, S.-S. Lee, M. Cribb, F. Zhang, X. Yang, C. Zhao, T. Takemura, K. Wang, X. Xia, Y. Yin, H. Zhang, J. Guo, P. M. Zhai, N. Sugimoto, S. S. Babu, and G. P. Brasseur, 2016: Aerosol and monsoon climate interactions over Asia. *Rev. Geophys.*, **54**, 866–929, doi:10.1002/2015RG000500.

Lindvall, J., and G. Svensson, 2014: The diurnal temperature range in the CMIP5 models. *Clim. Dyn.*, **44**, 405–421, doi:10.1007/s00382-014-2144-2.

Liu, L., Z. Li, X. Yang, H. Gong, C. Li, and A. Xiong, 2016: The long-term trend in the diurnal temperature range over Asia and its natural and anthropogenic causes. *J. Geophys. Res. Atmos.*, **121**, 3519–3533, doi:10.1002/2015JD024549.

Lobell, D. B., C. Bonfils, and P. B. Duffy, 2007: Climate change uncertainty for daily minimum and maximum temperatures: A model inter-comparison. *Geophys. Res. Lett.*, **34 (5)**, 1–5, doi: 10.1029/2006GL028726.

Makowski, K., E. B. Jaeger, M. Chiacchio, M. Wild, T. Ewen, and A. Ohmura, 2009: On the relationship between diurnal temperature range and surface solar radiation in Europe. *J. Geophys. Res. Atmos.*, **114 (7)**, 1–16, doi:10.1029/2008JD011104.

Makowski, K., M. Wild, and A. Ohmura, 2008: Diurnal temperature range over Europe between 1950 and 2005. *Atmos. Chem. Phys. Discuss.*, **8 (2)**, 7051–7084, doi:10.5194/acpd-8-7051-2008.

Ming, Y., V. Ramaswamy, and G. Chen, 2011: A model investigation of aerosol-induced changes in boreal winter extratropical circulation. *J. Clim.*, **24 (23)**, 6077–6091, doi:10.1175/2011JCLI4111.1.

Moore, G. W. K., 2013: Tibetan ice core evidence for an intensification of the East Asian jet stream since the 1870s. *Atmos. Sci. Lett.*, **14 (4)**, 235–242, doi:10.1002/asl2.445.

Morice, C. P., J. J. Kennedy, N. A. Rayner, and P. D. Jones, 2012: Quantifying uncertainties in global and regional temperature change using an ensemble of observational estimates: The HadCRUT4 data set. *J. Geophys. Res.*, **117 (D8)**, D08 101, doi:10.1029/2011JD017187.

Myhre, G., D. Shindell, F.-M. Bron, W. Collins, J. Fuglestvedt, J. Huang, D. Koch, J.-F. Lamarque, D. Lee, B. Mendoza, T. Nakajima, A. Robock, G. Stephens, T. Takemura, and H. Zhang, 2013: Anthropogenic and Natural Radiative Forcing. *Climate Change 2013: The Physical Science Basis. Contribution of Working Group I to the Fifth Assessment Report of the Intergovernmental Panel on Climate Change*, T. Stocker, D. Qin, G.-K. Plattner, M. Tignor, S. Allen, J. Boschung,

A. Nauels, Y. Xia, V. Bex, and P. Midgley, Eds., Cambridge University Press, Cambridge, United Kingdom and New York, NY, USA.

Acosta Navarro, J. C., V. Varma, I. Riipinen, Ø. Seland, A. Kirkevåg, H. Struthers, T. Iversen, H.-C. Hansson, and A. M. L. Ekman, 2016: Amplification of Arctic warming by past air pollution reductions in Europe. *Nat. Geosci.*, **9**, 277–281, doi:10.1038/NGEO2673.

Nicholson, S. E., 2013: The West African Sahel: A Review of Recent Studies on the Rainfall Regime and Its Interannual Variability. *ISRN Meteorol.*, **2013**, doi:10.1155/2013/453521.

Pausata, F. S. R., M. Gaetani, G. Messori, S. Kloster, and F. J. Dentener, 2014: The role of aerosol in altering North Atlantic atmospheric circulation in winter and air-quality feedbacks. *Atmos. Chem. Phys. Discuss.*, **14 (16)**, 22 477–22 506, doi:10.5194/acpd-14-22477-2014.

Pena-Ortiz, C., D. Gallego, P. Ribera, P. Ordonez, and M. Del Carmen Alvarez-Castro, 2013: Observed trends in the global jet stream characteristics during the second half of the 20th century. *J. Geophys. Res. Atmos.*, **118 (7)**, 2702–2713, doi:10.1002/jgrd.50305.

Polson, D., M. Bollasina, G. C. Hegerl, and L. J. Wilcox, 2014: Decreased monsoon precipitation in the Northern Hemisphere due to anthropogenic aerosols. *Geophys Res Lett*, **41 (16)**, 6023–6029, doi:10.1002/2014GL060811.

Ramanathan, V., P. J. Crutzen, J. T. Kiehl, and D. Rosenfeld, 2001: Aerosols, Climate, and the Hydrological Cycle. *Science*, **294**, 2119–2124, doi:10.1126/science.1064034.

Ribes, A., and L. Terray, 2013: Application of regularised optimal fingerprinting to attribution . Part II : application to global near-surface temperature. *Clim Dyn*, **41**, 2837–2853, doi:10.1007/s00382-013-1736-6.

Robock, A., and J. Mao, 1995: The volcanic signal in surface temperature observations. *J. Clim.*, **8 (5)**, 1086–1103, doi:10.1175/1520-0442(1995)008⟨1086:TVSIST⟩2.0.CO;2.

Rohde, R., R. A. Muller, R. Jacobsen, E. Muller, S. Perlmutter, A. Rosenfeld, J. Wurtele, D. Groom, and C. Wickham (2013a), A New Estimate of the Average Earth Surface Land Temperature Spanning 1753 to 2011, *Geoinfor Geostat*, *1*(1), 1–7, doi:10.4172/2327-4581.1000101.

Rohde, R., R. Muller, R. Jacobsen, S. Perlmutter, A. Rosenfeld, J. Wurtele, J. Curry, C. Wickham, and S. Mosher (2013b), Geostatistics : An Overview Berkeley Earth Temperature Averaging Process, *Geoinfor Geostat*, *1:2*, doi:10.4172/2327-4581.1000103.

Rotstayn, L. D., S. J. Jeffrey, M. a. Collier, S. M. Dravitzki, a. C. Hirst, J. I. Syktus, and K. K. Wong, 2012: Aerosol- and greenhouse gas-induced changes in summer rainfall and circulation in the Australasian region: a study using single-forcing climate simulations. *Atmos. Chem. Phys.*, **12 (14)**, 6377–6404, doi:10.5194/acp-12-6377-2012.

Rotstayn, L. D., and U. Lohmann, 2002: Tropical rainfall trends and the indirect aerosol effect. *J. Clim.*, **15 (15)**, 2103–2116, doi:10.1175/1520-0442(2002)015⟨2103:TRTATI⟩2.0.CO;2.

Saeed, S., N. Van Lipzig, W. A. Müller, F. Saeed, and D. Zanchettin, 2014: Influence of the circumglobal wave-train on European summer precipitation. *Clim. Dyn.*, **43 (1-2)**, 503–515, doi:10.1007/s00382-013-1871-0.

Schmidt, G. A., M. Kelley, L. Nazarenko, R. Ruedy, G. L. Russell, I. Aleinov, M. Bauer, S. E. Bauer, M. K. Bhat, R. Bleck, V. Canuto, Y.-H. Chen, Y. Cheng, T. L. Clune, A. D. Genio, R. D. Fainchtein, G. Faluvegi, J. E. Hansen, R. J. Healy, N. Y. Kiang, D. Koch, A. A. Lacis, A. N. Legrande, J. Lerner, K. K. Lo, E. E. Matthews, S. Menon, R. L. Miller, V. Oinas, A. O. Oloso, J. P. Perlwitz, M. J. Puma, W. M. Putman, D. Rind, A. Romanou, M. Sato, D. T. Shindell, S. Sun,

R. A. Syed, N. Tausnev, K. Tsigaridis, N. Unger, A. Voulgarakis, M.-S. Yao, and J. Zhang (2014), Configuration and assessment of the GISS ModelE2 contributions to the CMIP5 archive, *J. Adv. Model. Earth Syst.*, *6*, 141–184, doi:10.1002/2013MS000265.Received.

Schnur, R., and K. L. Hasselmann, 2005: Optimal filtering for Bayesian detection and attribution of climate change. *Clim. Dyn.*, **24 (1)**, 45–55, doi:10.1007/s00382-004-0456-3.

Schurer, A. P., and G. C. Hegerl, D. Polson, C. Morice, and S. F. B. Tett, Estimating the transient climate response from observed warming. *J Clim.*, submitted.

Shindell, D., M. Schulz, Y. Ming, T. Takemura, G. Faluvegi, and V. Ramaswamy, 2010: Spatial scales of climate response to inhomogeneous radiative forcing. *J. Geophys. Res.*, **115 (D19)**, D19 110, doi:10.1029/2010JD014108.

Stjern, C. W., and J. E. Kristjánsson, 2015: Contrasting Influences of Recent Aerosol Changes on Clouds and Precipitation in Europe and East Asia. *J Clim.*, **28**, 8770–8790, doi:10.1175/JCLI-D-14-00837.1.

Stjern, C. W., A. Stohl, and J. E. Kristjánsson, 2011: Have aerosols affected trends in visibility and precipitation in Europe? *J. Geophys. Res.*, **116 (D02212)**, 1–15, doi:10.1029/2010JD014603.

von Storch, H., and F. W. Zwiers, 1999: *Statistical Analysis in Climate Research*. Cambridge University Press, Cambridge, United Kingdom and New York, NY, USA and Port Melbourne, Australia, doi:0511010184

Stott, P. A., and G. S. Jones, 2012: Observed 21st century temperatures further constrain likely rates of future warming. *Atmos. Sci. Let.*, **13**, 151–156, doi:10.1002/asl.383.

Strong, C., and R. E. Davis, 2007: Winter jet stream trends over the Northern Hemisphere. *Q. J. R. Meteorol. Soc.*, **133**, 2109–2115, doi:10.1002/qj.171.

885 Tao, L., Y. Hu, and J. Liu, 2016: Anthropogenic forcing on the Hadley circulation in CMIP5
886 simulations. *Clim. Dyn.*, **46 (9-10)**, 3337–3350, doi:10.1007/s00382-015-2772-1.

887 Taylor, K. E., R. J. Stouffer, and G. A. Meehl, 2012: An Overview of CMIP5 and the Experiment
888 Design. *Bull. Am. Meteorol. Soc.*, **93 (4)**, 485–498, doi:10.1175/BAMS-D-11-00094.1.

889 Thorne, P. W., M. G. Donat, R. J. H. Dunn, C. N. Williams, L. V. Alexander, J. Caesar, I. Durre,
890 I. Harris, Z. Hausfather, P. D. Jones, M. J. Menne, R. Rohde, R. S. Vose, R. Davy, J. H. Law-
891 rimore, T. C. Peterson, and J. J. Rennie (2016), Reassessing changes in diurnal temperature
892 range: Intercomparison and evaluation of existing global data set estimates, *J. Geophys. Res.*
893 *Atmos.*, *121*, 5138–5158, doi:10.1002/2015JD024584.

894 Twomey, S., 1977: The Influence of Pollution on the Shortwave Albedo of Clouds. *J. Atmos. Sci.*,
895 **34**, 1149–1152, doi:10.1175/1520-0469(1977)034⟨1149:TIOPOT⟩2.0.CO;2.

896 Undorf, S., D. Polson, M. Bollasina, Y. Ming, A. Schurer, and G. C. Hegerl, 2018: Detectable
897 impact of local and remote anthropogenic aerosols on the 20th century changes of West African
898 and South Asian monsoon precipitation. *J. Geophys. Res. Atmos.*, doi:10.1029/2017JD027711.

899 von Salzen, K., J. F. Scinocca, N. A. McFarlane, J. Li, J. N. S. Cole, D. Plummer, D. Verseghy,
900 M. C. Reader, X. Ma, M. Lazare, and L. Solheim (2013), The Canadian Fourth Generation
901 Atmospheric Global Climate Model (CanAM4). Part I: Representation of Physical Processes,
902 *Atmos.-Ocean*, *51*(1), 104–125, doi:10.1080/07055900.2012.755610.

903 Wang, H., S. P. Xie, and Q. Liu (2016), Comparison of climate response to anthropogenic aerosol
904 versus greenhouse gas forcing: Distinct patterns, *J. Climate*, *29*(14), 5175–5188, doi:10.1175/
905 JCLI-D-16-0106.1.

Wilcox, L. J., E. J. Highwood, B. B. B. Booth, and K. S. Carslaw, 2015: Quantifying sources of inter-model diversity in the cloud albedo effect. *Geophys. Res. Lett.*, **42**, 1568–1575, doi: 10.1002/2015GL063301.

Wilcox, L. J., E. J. Highwood, and N. J. Dunstone, 2013: The influence of anthropogenic aerosol on multi-decadal variations of historical global climate. *Environ. Res. Lett.*, **8 (2)**, 24 033, doi: 10.1088/1748-9326/8/2/024033.

Wild, M., A. Ohmura, and K. Makowski, 2007: Impact of global dimming and brightening on global warming. *Geophys. Res. Lett.*, **34 (4)**, 1–4, doi:10.1029/2006GL028031.

Yadav, R. K., 2017: On the relationship between east equatorial Atlantic SST and ISM through Eurasian wave. *Clim Dyn*, **48**, 281–295, doi:10.1007/s00382-016-3074-y.

Zelinka, M. D., T. Andrews, P. M. Forster, and K. E. Taylor, 2014: Quantifying components of aerosol-cloud-radiation interactions in climate models. *J Geophys Res Atmos*, **119 (12)**, 7599–7615, doi:10.1002/2014JD021710.

LIST OF TABLES

TABLE 1. CMIP5 models used in this study. The Table includes the number of ensemble members available for aerosol-only simulations as well as whether each model includes any representation of the first and second indirect aerosol effects. An overview of the experiment design is given in Taylor et al. (2012).

Institute ID	Model Name	#ens. members	aerosol indirect effects		Reference
			1st	2nd	
CCCMA	CanESM2	5	x	-	von Salzen et al. (2013)
CSIRO-QCCCE	CSIRO-Mk3.6.0	5	x	x	Jeffrey et al. (2013)
IPSL	IPSL-CM5A-LR	1	x	-	Dufresne et al. (2013)
MOHC	HadGEM2-ES	4	x	x	Collins et al. (2011)
NASA GISS	GISS-E2-R	5	x	x	Schmidt et al. (2014)
NCC	NorESM1-M	1	x	x	Iversen et al. (2013)
NOAA GFDL	GFDL-CM3	3	x	x	Donner et al. (2011)

LIST OF FIGURES

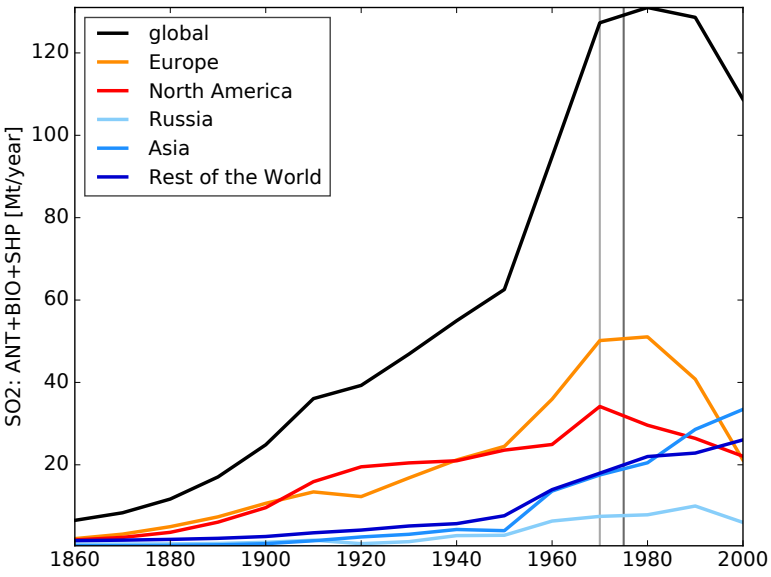

FIG. 1. Total SO2 emissions (kg/s) during boreal summer (JJA) from all sectors (anthropogenic, biomass burning, and shipping) from Europe (EU) (30-75°N, -15-45°E; orange), North America (NA) (15-75°N, 135-60°W; red), eastern Russia (RU) (45-75°N, 45-180°E; light blue), Asia (0-45°N, 60-150°E; medium blue), and the remaining parts of the globe (dark blue). Global emissions are also shown (black). The areas are chosen based on their emission time series, and do not conform strictly to political or geographical boundaries. NA, EU, and RU are similar to the respective Tier 1 regions from the Hemispheric Transport of Air Pollution 2 experiments (Koffi et al., 2016), but include for convenience other parts with negligible emissions (Arctic regions in NA, EU, and RU; northern Mexico in NA; Mongolia and Kazakhstan in RU). The Asian region includes mainly India, most of China, Japan, and southern Central Asia. The vertical lines indicate the year dividing the first and second time period for which trends are calculated: 1970 (light gray) for emissions (which are decadal), and 1975 for simulated variables (dark gray). Data from Lamarque et al. (2010).

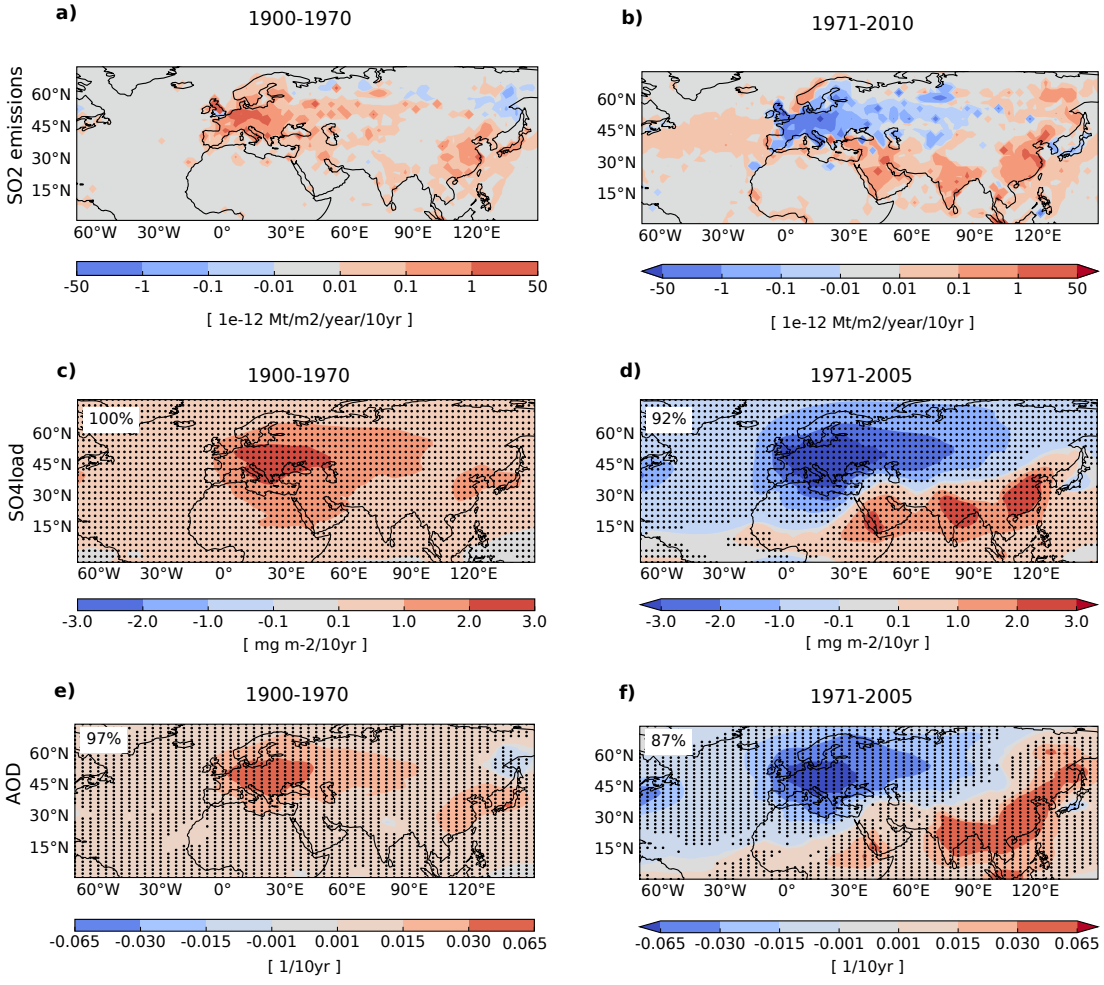

1024 FIG. 2. Linear trends of JJA (top) total SO2 emissions (Mt/m^2/year/decade) from all sectors, (middle) column-
1025 integrated sulphate loading (mg/m^2/decade), and (bottom) AOD (1/decade) during (left) 1900-1970 and (right)
1026 (b) 1971-2010 and (d,f) 1971-2005. Emission data are decadal, so we use 1970 here instead of 1975 as in later
1027 figures. For sulphate loading and AOD, the multi-model mean (MMM) of the aerosol-only simulations from
1028 the models listed Tab. 1 is shown except for (c-d) HadGEM2-ES and (e-f) CanESM2, respectively, due to data
1029 unavailability. Stippling indicates where at least 5 out of the 6 models' ensemble means agree on sign, and
1030 the fraction of stippled grid points within 0-90°N, -30-120°E is given in the top left corner. Trends in the all-
1031 forcing ensemble are very similar (not shown). Data from Lamarque et al. (2010) (emissions) and Taylor et al.
1032 (2012) (CMIP5). Note that trends during the second period exceed the colorbar range, as indicated by triangular
1033 colorbar ends.

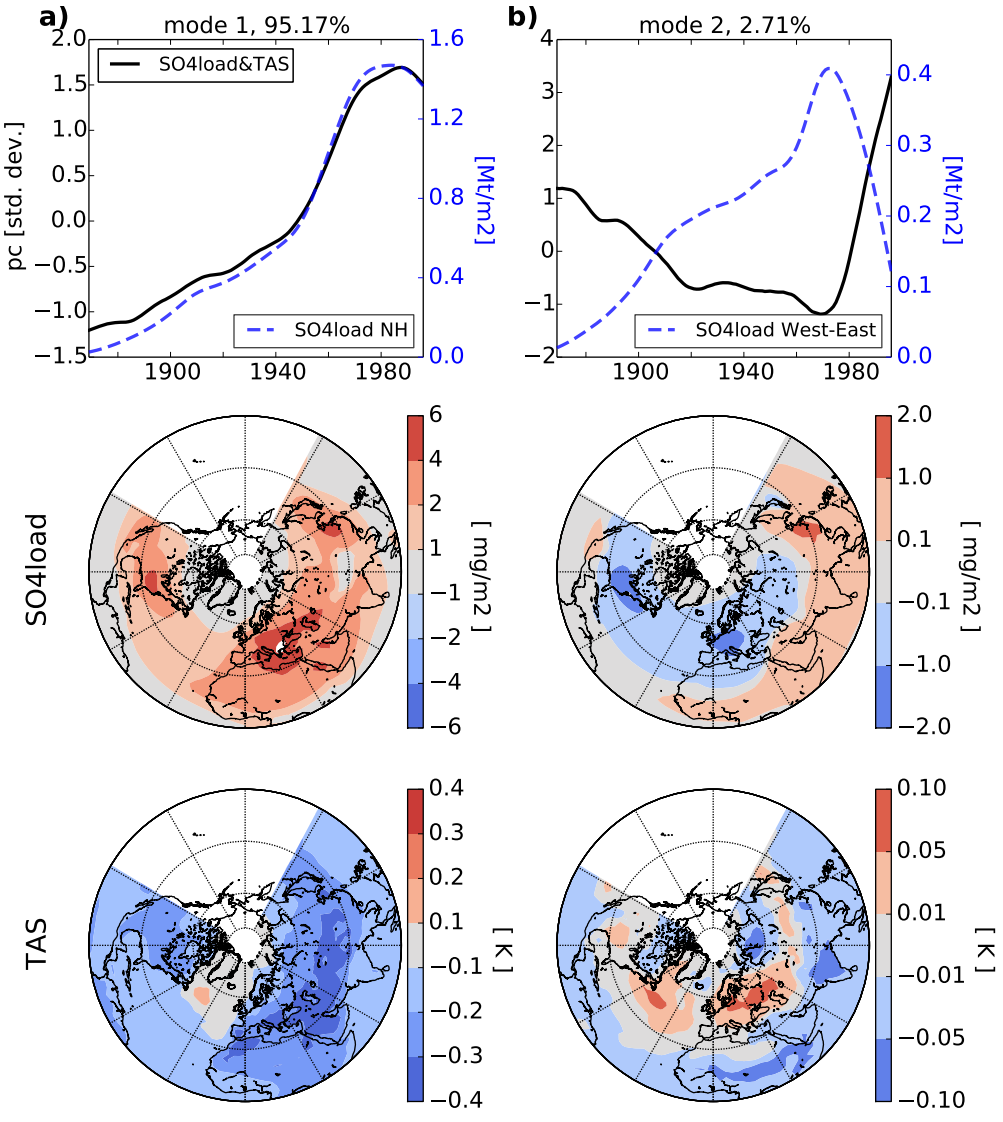

FIG. 3. Joint EOF analysis for JJA sulphate loading (SO4load) and near-surface temperature (TAS) from the multi-model mean of the aerosol-only CMIP5 simulations. The (top) principal components of the (a) first and (b) second mode are shown along with the respective patterns for (middle) SO4load and (bottom) TAS. For comparison, the (a) total SO4load over the northern hemisphere and (b) difference between SO4load over a western (NAEU) region (the sum of 20-90°N, -130-0°E; 30-90°N, 0-30°E; and 45-90°N, 30-60°E) and an eastern region (0-45°N, 30-135°E) are also shown (blue, dashed lines). The models used are those in Tab. 1 except for HadGEM2-ES (no data available; separate EOFs show the other results are not sensitive to the inclusion of this model (not shown)). We apply a 11-7 year filter prior to the analysis.

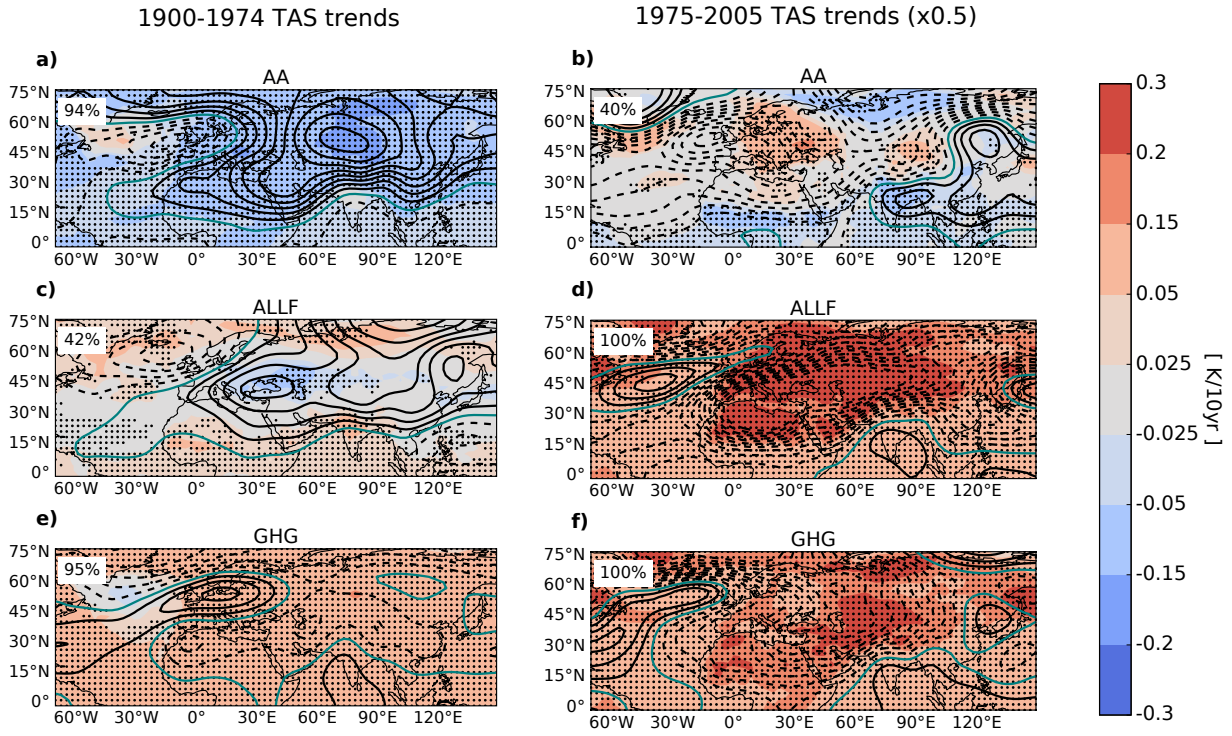

1042 FIG. 4. Linear trends in JJA near-surface temperature (TAS, color shading, in K/decade, and sea level pressure
1043 (SLP, contour lines, Pa/decade) during (left) 1900-1974 and (right) 1975-2005 for the multi-model mean of the
1044 (top) AA, (middle) ALLF, and (bottom) GHG simulations. Stippling indicates where at least 6 out of the 7
1045 models' ensemble means agree on sign for TAS, and the fraction of stippled grid points within 0-90°N, -30-
1046 120°E is given in the top left corner. Dashed contour lines indicate negative sea level pressure trends; the zero
1047 contour line is drawn in turquoise. The contour interval is 1.25 Pa/10yr. See Fig. S7 for the robustness of the
1048 SLP trends. Note that both temperature and SLP trends during the second period are scaled by 1/2 for easier
1049 comparison with those during the first period.

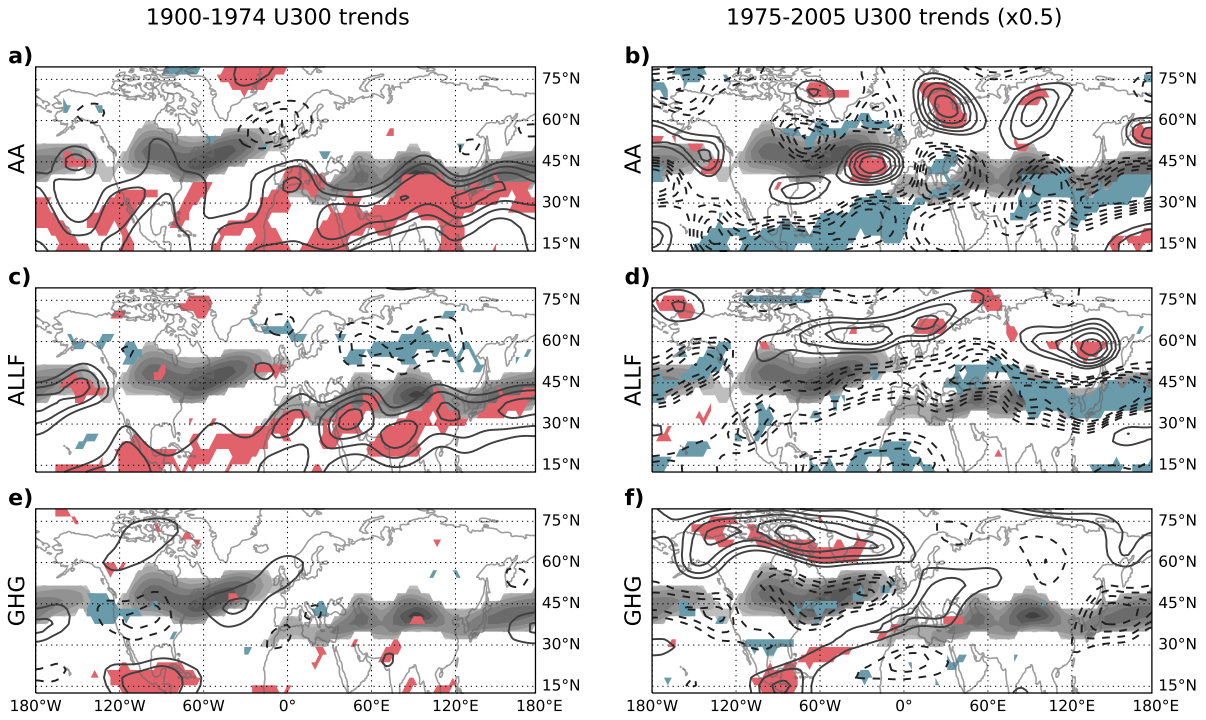

FIG. 5. Linear trends in JJA zonal wind at 300 hPa (U300, contour lines) during (left) 1900-1974 and (right) 1975-2005 for the multi-model mean of the (top) AA, (middle) ALLF, and (bottom) GHG simulations. Dashed contour lines indicate negative trends. The contour interval is 0.02 m/s/decade. The 0.00 and $\pm$0.02 contours are not displayed for clarity. Gray shading indicates where the climatological zonal wind speed at 300 hPa exceeds 12.5 m/s as a rough estimate of the jet stream position. Coloring (red for positive trends, blue for negative ones) indicates where at least 6 out of the 7 models' ensemble means agree on sign. Note that trends during the second period are scaled by 1/2 for easier comparison with those during the first period.

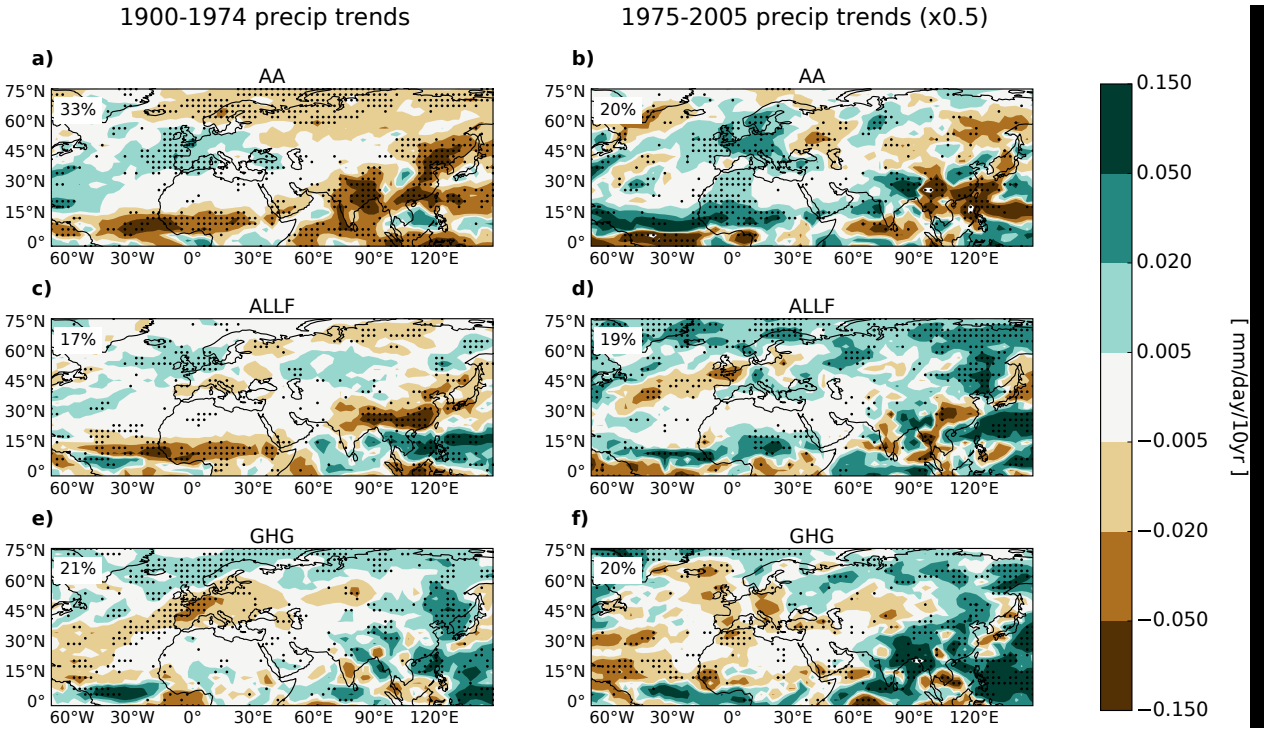

1057 FIG. 6. Linear trends in precipitation (precip, in mm/day/decade) for JJA during (left) 1900-1974 and (right)
1058 1975-2005 for the multi-model mean of the (top) AA, (middle) ALLF, and (bottom) GHG simulations. Stippling
1059 indicates where at least 6 out of the 7 models' ensemble means agree on sign, and the fraction of stippled grid
1060 points within 0-90°N, -30-120°E is given in the top left corner. Note that trends during the second period are
1061 scaled by 1/2 for easier comparison with those during the first period.

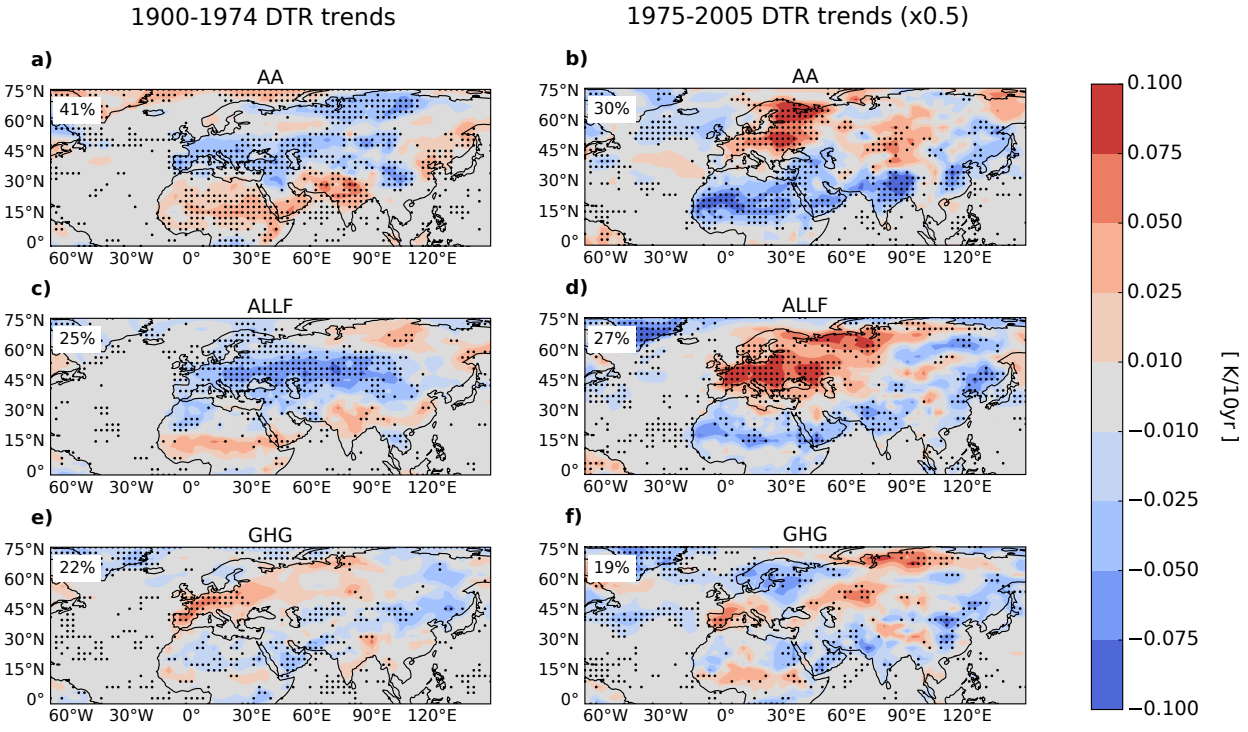

1062 FIG. 7. Linear trends in DTR (in K/decade) for JJA during (left) 1900-1974 and (right) 1975-2005 for the
1063 multi-model mean of the (top) AA, (middle) ALLF, and (bottom) GHG simulations for the models listed in Tab.
1064 1; for AA, no HadGEM2-ES data is available, thus the MMM of the remaining six models is shown. Stippling
1065 indicates where at least 6 out of the 7 (ALLF, GHG) or 5 out of the 6 (AA) models' ensemble means agree on
1066 sign, and the fraction of stippled grid points within 0-90°N, -30-120°E is given in the top left corner. Note that
1067 trends during the second period are scaled by 1/2 for easier comparison with those during the first period.

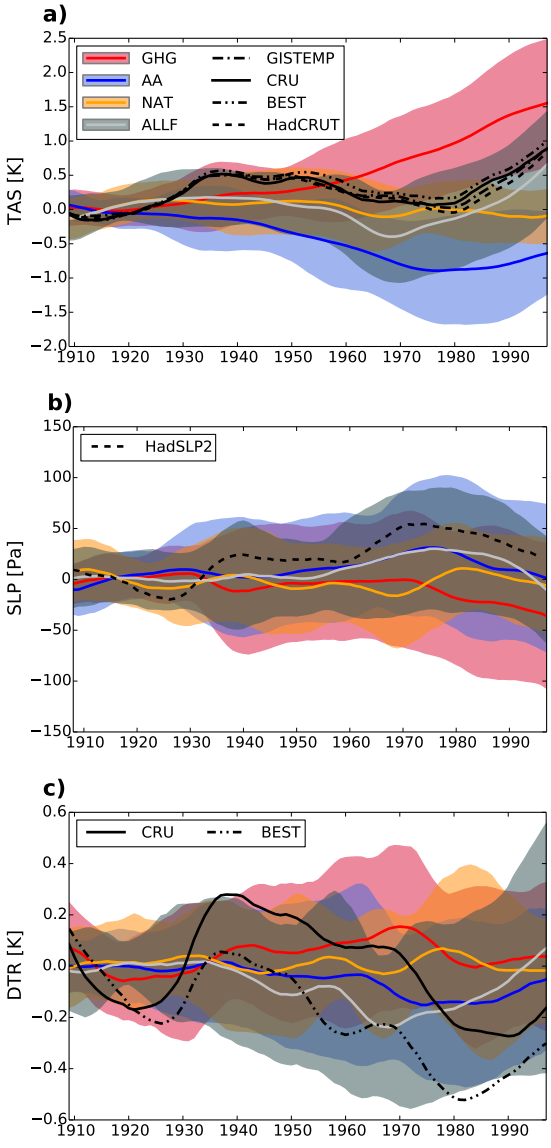

FIG. 8. Comparison with observations over Europe (35-60°N, 0-60°E): Time series of area-mean JJA a) near-surface temperature (TAS, K), b) sea level pressure (SLP, Pa), and c) diurnal temperature range (DTR, K). Observations (black lines) are shown as well as the CMIP5 multi-model mean for single-forcing (AA in blue, GHG in red, NAT in yellow) and all-forcing simulations (ALLF in gray) along with the range of 1.96 standard deviations of the individual model simulations (shading). The CMIP5 data for TAS and DTR are masked to the coverage of the respective CRU dataset. All data are temporally smoothed with a 11-7 year filter, and anomalies with respect to 1901-1930 are plotted. For DTR, no HadGEM2-ES data is available, thus the MMM of the remaining six models is shown.

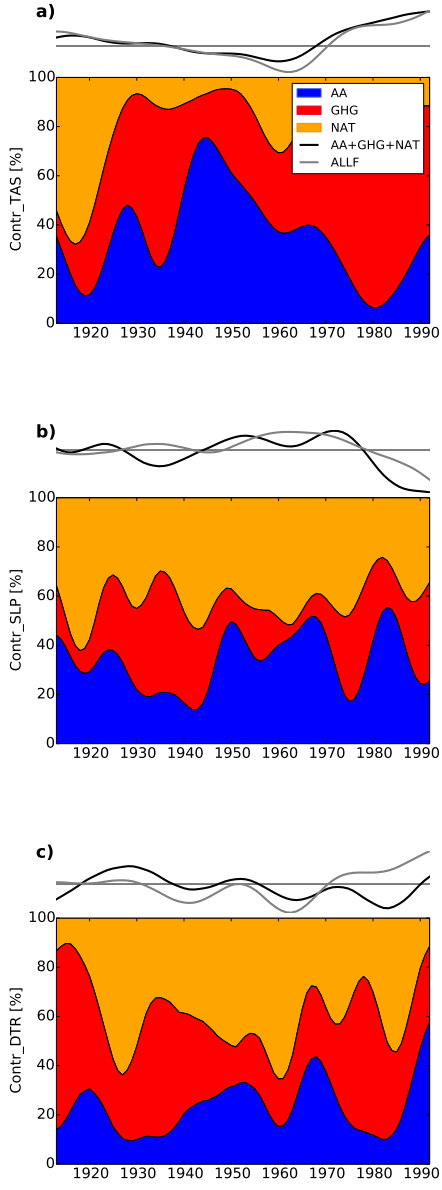

FIG. 9. Estimates of the contribution of each single forcing on the inter-decadal variability of a) near-surface temperature (TAS, %), b) sea level pressure (SLP, %), and c) diurnal temperature range (DTR, %) for the European region as in Fig. 8 (here the data are not masked to the observational coverage). At the top of each panel, the instantaneous gradient of the MMM all-forcing time series (gray) and the sum of the gradients of the MMM single-forcing time series (black) are shown. At the bottom of each panel, the contributions from GHG (red), AA (blue), and NAT (yellow) are shown, derived by taking the gradient of the ensemble-mean time series for each of these forcing experiments and dividing their magnitudes by the sum of all these gradient magnitudes. All time series are temporally smoothed with a 11-7 year filter prior to the analysis and further smoothed (7-5 year filter) for plotting.